A new adaptive switching median filter for impulse noise reduction with pre-detection based on evidential reasoning

Zhe Zhang, Deqiang Han, Jean Dezert, Yi Yang

A new adaptive switching median filter for impulse noise reduction with pre-detection based on evidential reasoning

Zhe Zhang[a], Deqiang Han[a,*], Jean Dezert[b], Yi Yang[c]

[a] *MOE KLINNS Lab, Institute of Integrated Automation, School of Electronic and Information Engineering, Xi'an Jiaotong University, Xi'an 710049, China*
[b] *ONERA, The French Aerospace Lab, Chemin de la Hunière, Palaiseau F-91761, France*
[c] *SKLSVMS, School of Aerospace, Xi'an Jiaotong University, Xi'an 710049, China*

Image denoising is a fundamental problem in image processing. The switching filtering is a popular approach to reduce the impulse noise. It faces two challenges including the impulse noise detection and filter design. The traditional detection methods based on single criterion or multiple criteria encounter uncertainty problems and produce many miss-detections and false alarms, especially when the image is severely corrupted. In this paper, the uncertainties encountered in the impulse noise detection are addressed using the theory of belief functions, and a multi-criteria detection strategy for the impulse noise based on evidential reasoning is proposed. Based on the pre-detection, an adaptive median filter is designed, which adaptively determines the size of the filtering window according to the estimated global noise density and the degree of local corruption. Experimental results and related analyses show that our proposed image denoising method for the impulse noise has superior performance compared with several state-of-the-art denoising methods.

1. Introduction

Digital images can be corrupted by various types of noise during the image acquisition and transmission. The impulse noise is one of the most common types, which is encountered in cases with quick transients, e.g., faulty switching during imaging [1]. The intensity of a pixel corrupted by the impulse noise tends to be much higher or lower than those of its uncorrupted neighbors. The impulse noise dramatically influences the image quality and makes images unsuitable for subsequent human understanding or image processing such as the edge detection [2], segmentation [3], object recognition [4], image analysis [5] and image understanding [6].

Till now, the impulse noise reduction problem has not been well solved and has attracted extensive research interests. The median filtering is the most popular approaches for the impulse noise reduction. The standard median (SM) filter [7] replaces the target pixel's intensity by the median of intensities of its neighbors. Various modifications of the SM filter have been proposed, such as the weighted median (WM) filter [8] and the center weighted median (CWM) filter [9]. However, all these filters apply the median operations to each pixel ignoring whether the target pixel is corrupted or not. This might destroy the details contributed from uncorrupted pixels and lead to image quality degradation. To deal with this problem, switching median filters [10] were proposed, which introduce the noise detection prior to the filtering. Since only the corrupted pixels will be filtered and the uncorrupted pixels remain intact, more details can be preserved and better filtering performance can be achieved if the pre-detection result is accurate enough.

In recent years, sparse representation (SR) [11] is widely used in image denoising [12–14], especially for Gaussian noise. For the impulse noise, the noise detector is incorporated into SR model and the weighted dictionary learning method was proposed for impulse noise denoising [15–17]. Both median filtering and SR based method face the challenge of noise detector designing.

There have emerged two major criteria for the impulse noise detection including the extreme property and discontinuity property. Some detectors only use a single criterion, which may involve some uncertainty problems. For example, the boundary discriminative noise detection (BDND) [18] and the efficient improvements on the BDND (IBDND) [19] use the criterion of extreme property. Both algorithms label a pixel as the noise if it is assigned to the low-intensity range or high-intensity range according to the histogram distribution in a local window centered at that given pixel. However, these detectors easily lead to false alarms since not all the pixels with low-intensity or high-intensity are noise. There are

* Corresponding author.
E-mail addresses: zhezhang@stu.xjtu.edu.cn (Z. Zhang), deqhan@mail.xjtu.edu.cn (D. Han), jean.dezert@onera.fr (J. Dezert), jiafeiyy@mail.xjtu.edu.cn (Y. Yang).

other detectors that only use the criterion of discontinuity property. Such detectors can be found in the adaptive impulse detection using center-weighted median (ACWM) filter [20], directional weighted median (DWM) filter [21], contrast enhancement-based (CEF) filter [22], adaptive switching median (ASWM) filter [23], weighted couple sparse representation (WCSR) model [24] and the denoising framework combining the detection mechanism based on the robust outlyingness ratio with the NL-means (ROR-NLM) [25]. They label a pixel as the noise if its similarity with its neighbors is lower than a preset threshold. However, when the noise density is high, the impulse noise pixels might not show the discontinuity property since there are too many noise pixels in their neighbors. Since pixels with extreme or discontinuity property may not always be the noise, the detectors based on a single criterion will involve uncertainty problems and tend to yield incorrect detection results. Both criteria have their own rationalities; however, they are one-sided. It should be better to jointly use them when detecting the impulse noise. Therefore, some approaches using the above two criteria jointly have been proposed, e.g., the detector in noise adaptive soft-switching median (NASM) filter [26] and the detector based on the cloud model (CM) [27]. These two-step detection methods first recognize the suspected noise pixels using the extreme criterion, and then distinguish the noise pixels from the suspected noise pixels using the discontinuity criterion. However, they can easily produce miss-detections when some noise pixels are not detected as the suspected noise in the first step. Therefore, the two-step type joint use is not preferred.

To deal with the uncertainties encountered in the impulse noise detection and avoid the drawbacks of the two-step-type joint use of detection criteria, in this paper, a new detection approach for the impulse noise is proposed, which uses the two criteria simultaneously based on the theory of belief functions [28]. In our detection approach, the extreme property is described using the interval data distance between the target pixel's intensity and the intensity range of the whole noisy image (expressed as an interval number). The discontinuity property is described using the rank-ordered absolute differences (ROAD) statistic [29]. The uncertainty problem encountered in the impulse noise detection, e.g., pixels with extreme or discontinuity property may not always be the noise, are modeled by belief functions and are further handled through the evidence combination.

The impulse noise detector implementation is the main work of this paper. Based on the detection result, an adaptive median filter is designed, which adaptively determines the size of filtering window according to the estimated global noise density and local corrupted degree. Experimental results show that our proposed adaptive switching median filter with pre-detection based on evidential reasoning (ASMF-DBER) has superior performance compared with several state-of-the-air switch median filters and the SR based method.

2. Basis of impulse noise and uncertainty problems encountered in impulse noise detection

2.1. Impulse noise model

When an image is corrupted by the impulse noise, some pixels are changed and their intensities are extremely high or extremely low. We use the same impulse noise model as used in BDND [18]. Assume that the noise pixels take values in two fixed sets $S_1 = \{0, 1, \ldots, \alpha\}$ and $S_2 = \{255 - \alpha, 255 - (\alpha - 1), \ldots, 255\}$ for an 8-bit monochrome image. Let $s_{i,j}$ and $x_{i,j}$ be the pixels' intensities at location (i, j) in the original and noisy images, respectively. Let $n_{i,j}$ be the noise which is independent of $s_{i,j}$ and corresponds to a random value uniformly distributed in the set S_1 and S_2. Let p denote the probability that a pixel is corrupted. The probability mass function (pmf) [30] of $x_{i,j}$ is given by

$$P(x_{i,j}) = \begin{cases} p, & \text{for } x_{i,j} = n_{i,j}, \\ 1 - p, & \text{for } x_{i,j} = s_{i,j}. \end{cases} \tag{1}$$

Specially, if $\alpha = 0$, the intensities of noise pixels can only take the two extreme values 0 or 255. This type of impulse noise is also called the salt-and-pepper noise. Since $n_{i,j}$ is independent of $s_{i,j}$, it is possible that $n_{i,j} = s_{i,j}$. This kind of pixel should be regarded as uncorrupted.

2.2. Uncertainties encountered in impulse noise detection

The impulse noise has two properties:

(a) *Extreme property*: The intensity of an impulse noise pixel is usually an extreme value (0 or 255) or close to an extreme value.
(b) *Discontinuity property*: The intensity of an impulse noise pixel tends to be much higher or lower than those of its neighbors.

These two properties are often used as detection criteria for the impulse noise. Some detectors only use one of the criteria:

(a) Detectors based on the criterion of extreme property: These detectors label a pixel as the noise, if it is assigned to the low-intensity range or high-intensity range according to the histogram distribution in a local window centered at that pixel, e.g., BDND [18] and IBDND [19] detectors.
(b) Detectors based on the criterion of discontinuity property: These detectors label a pixel as the noise, if its dissimilarity with its neighbors is larger than a preset threshold, such as ACWM [20], DWM [21], CEF [22], ASWM [23], ROR-NLM [25] and WCSR [24].

However, such single criterion based detectors may involve the following uncertainty problems:

(a) Uncertainty in extreme criterion: Some signal pixels may also be detected as the noise, since their intensities are very close to extreme values, e.g., some edge pixels and texture pixels. Moreover, in some bright or dark area, the intensity range of signal pixels may overlap with that of the impulse noise pixels. Therefore, when using the extreme criterion alone, it is uncertain to judge those signal pixels with extreme property to be the impulse noise or not.
(b) Uncertainty in discontinuity criterion: The discontinuity property of the impulse noise pixels becomes weaker with the increase of noise density since there are many noise pixels in their neighbors. At the same time, some signal pixels may show discontinuity. Therefore, with only the discontinuity criterion, it is uncertain to judge a pixel to be the impulse noise or not.

Due to these uncertainties, the single criterion based detectors are to some extent one-sided and tend to yield incorrect detection results. Hence, it should be better to jointly use the two criteria to implement a more comprehensive detection.

Some two-step detection methods, like NASM [26] and CM [27], jointly use these two criteria in two consecutive steps. They first recognize suspected noise pixels according to the extreme criterion, and then distinguish noise pixels from suspected noise pixels according to the discontinuity criterion, as illustrated in Fig. 1. In the first step, only using the extreme criterion, some noise pixels may not be detected as the suspected noise and therefore are miss-detected straightly. These miss-detected pixels will not undergo the filtering so that these two-step methods can easily lead to poor noise-reduction capabilities. Therefore, when detecting the

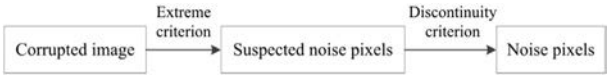

Fig. 1. The two-step detection method.

impulse noise, it should be better to use these two criteria simultaneously, but not in two consecutive steps.

To deal with these uncertainties encountered in the single criterion based detections and to implement a more comprehensive detection by using these two criteria simultaneously, we propose an evidential reasoning based impulse noise detection approach thanks to the ability of belief functions to model uncertainty and for reasoning under uncertainty. The theory of belief functions [28] are briefly recalled first below.

3. Impulse noise detection based on evidential reasoning

3.1. Basic of evidence theory

The theory of belief functions, also called Dempster–Shafer evidence theory (DST) [28], is a theoretical framework for uncertainty modeling and reasoning.

In DST, elements in the frame of discernment (FOD) $\Theta = \{\theta_1, \theta_2, \ldots, \theta_l\}$ are mutually exclusive and exhaustive. The power set 2^{Θ} of the FOD Θ is the set of all subsets of Θ. Define a function m from 2^{Θ} to [0, 1] as a basic belief assignment (BBA, also called a mass function) satisfying

$$\sum_{A\subseteq\Theta} m(A) = 1,\ m(\emptyset) = 0 \tag{2}$$

$m(A)$ depicts the evidence support to the proposition A. If $m(A) > 0$, A is called a focal element.

The plausibility function (Pl) and belief function (Bel) are defined as:

$$Pl(A) = \sum_{A\cap B\neq\emptyset} m(B) \tag{3}$$

$$Bel(A) = \sum_{B\subseteq A} m(B) \tag{4}$$

The belief interval [28,31] $[Bel(A), Pl(A)]$ represents the imprecision of the support to the proposition A.

Dempster's rule of combination [28], which is used for combining two distinct pieces of evidence, is defined as

$$(m_1 \oplus m_2)(A) = \begin{cases} 0, & A = \emptyset \\ \dfrac{1}{1-K} \displaystyle\sum_{B\cap C=A} m_1(B)m_2(C), & A \neq \emptyset \end{cases} \tag{5}$$

where $K = \sum_{B\cap C=\emptyset} m_1(B)m_2(C)$ represents the total conflict or contradictory mass assignments.

For a probabilistic decision-making, Smets defined the pignistic probability transformation [32] to transform a BBA into a probability measure BetP:

$$\mathrm{BetP}(\theta_i) \triangleq \sum_{\theta_i\in A} \frac{m(A)}{|A|} \quad \forall\theta_i \in \Theta \tag{6}$$

where $|A|$ denotes the cardinality of A. The decision is made by choosing the element in FOD which has the highest BetP value. Note that there are still other probability transformations of BBA, see [33] for details.

3.2. Evidential modeling for uncertainties and fusion based detection

To deal with the uncertainties encountered in the impulse noise detection, we propose a detection method based on evidential reasoning, which uses the extreme criterion and discontinuity criterion simultaneously. The flow chart of the detection algorithm is illustrated in Fig. 2.

Here we propose two methods for uncertainties modeling. One proposed method models the uncertainties of extreme criterion and discontinuity criterion with two BBAs, respectively (denoted by method I). The other proposed method treats this impulse noise detection with two criteria as a multi-criteria decision making problem, and uses cautious ordered weighted averaging with evidential reasoning (COWA-ER) method [34] to generate BBAs (denoted by method II). In both methods, we use the distance of interval numbers to describe the extreme property and use the rank-ordered absolute differences (ROAD) statistic [29] to describe the discontinuity property.

3.2.1. Evidential modeling method I and fusion based detection

1) *Evidential modeling for the uncertainty in extreme criterion* According to the extreme property of the impulse noise, the intensity of an impulse noise pixel must be an extreme value or close to an extreme value.

Since all of the pixels' intensities in an image are within a range ([0, 255] for an 8-bit image), the intensity information of an image can be represented by an interval number. An interval number $\tilde{a}$ in $\mathbb{R}$ is a set of real numbers that lie between two real numbers, i.e., $\tilde{a} = [a_1, a_2] = \{x | a_1 \le x \le a_2\}$, $a_1, a_2 \in \mathbb{R}$ and $a_1 \le a_2$. The intensity information of an image can be expressed as an interval number $\tilde{I} = [I_{\min}, I_{\max}]$, where $I_{\min}$ and $I_{\max}$ denote the minimum and maximum intensities of the image, respectively. Furthermore, a single pixel's intensity x can also be viewed as an interval number $[x, x]$, whose upper bound and lower bound are equal.

The distance of interval numbers is a measure of dissimilarity between interval numbers. Here we use it to describe the closeness between a pixel's intensity and the extreme values. Various types of distance for interval numbers [35] have been proposed. Here, we use the following strict distance metric. Given two interval numbers $\tilde{a} = [a_1, a_2]$ and $\tilde{b} = [b_1, b_2]$, the distance between $\tilde{a}$ and $\tilde{b}$ is defined as:

$$d(\tilde{a}, \tilde{b}) = \sqrt{\left[\frac{(a_1+a_2)-(b_1+b_2)}{2}\right]^2 + \frac{1}{3}\left[\frac{(a_2-a_1)-(b_2-b_1)}{2}\right]^2}. \tag{7}$$

According to (7), the distance between $\tilde{I}$ and $[x, x]$, which describes the closeness between a pixel's intensity x and the extreme values, $I_{\min}$ and $I_{\max}$, is:

$$d(\tilde{I}, [x, x]) = \sqrt{\left(\frac{I_{\min}+I_{\max}}{2} - x\right)^2 + \frac{(I_{\max}-I_{\min})^2}{12}}. \tag{8}$$

Here, x takes values in the interval $[I_{\min}, I_{\max}]$. An illustration of $d(\tilde{I}, [x, x])$ is shown in Fig. 3, where the intensity range of the image is set as [0, 255]. When x takes the median of [0, 255], i.e., 127 or 128, $d(\tilde{I}, [x, x])$ reaches the minimum value. The closer between x and the extreme value, e.g., 0 or 255, the higher the value of $d(\tilde{I}, [x, x])$. Thus, $d(\tilde{I}, [x, x])$ can be used to describe the extreme property.

Suppose that the only possible type of the noise existing in the given image is the impulse noise. The pixel whose intensity is far from the extreme values must be the signal, but the pixel whose intensity is close to an extreme value may not be the noise. For example, in some bright or dark area, the intensity range of signal pixels may overlap with that of the impulse noise pixels. Here, we use the belief function to describe this uncertainty.

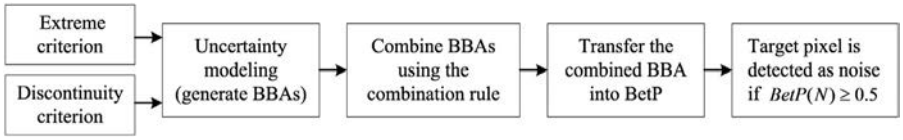

Fig. 2. Noise detection algorithm based on evidential reasoning.

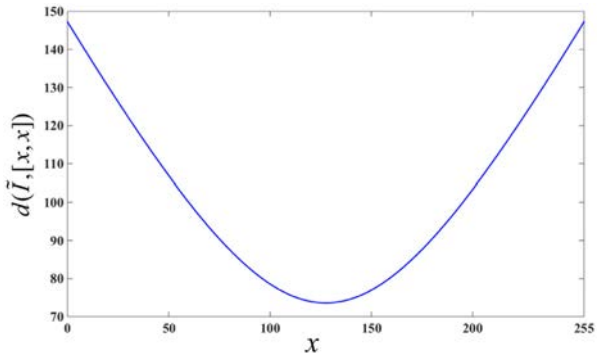

Fig. 3. An illustration of $d(\tilde{I},[x,x])$.

We set a detection window with a size of $w_D \times w_D$ centered at the given pixel at (i, j):

$$W_D(i,j) = \{x_{i-s,j-t} | -(w_D-1)/2 \leq s,t \leq (w_D-1)/2\} \tag{9}$$

where $x_{i-s,j-t}$ is the intensity of the pixel at $(i-s, j-t)$.

We focus on two distances in W_D:

(a) d_c denotes the distance between the center pixel's intensity and the interval number $\tilde{I}$, where $\tilde{I}$ expresses the intensity range of the pixels in the whole image.
(b) d_0 denotes the minimum distance in W_D between a pixel's intensity and $\tilde{I}$, where the pixel is the one whose intensity is the farthest one in W_D from the extreme values. Thus, this pixel is most unlikely to be the noise in W_D according to the extreme criterion.

We also focus on another two distances in the whole image:

(a) d_{ext} denotes distance between $\tilde{I}$ and the extreme value: $I_{\min}$ or $I_{\max}$. It is the maximum distance in the image between a pixel's intensity and $\tilde{I}$. If a pixel's intensity is close to the extreme value, its distance to $\tilde{I}$ is close to d_{ext}.
(b) d_{med} denotes distance between $\tilde{I}$ and the median of $\tilde{I}$. It is the minimum possible distance in the image between a pixel's intensity and $\tilde{I}$. If a pixel's intensity is much far from the extreme values, its distance to $\tilde{I}$ is close to d_{med}.

Finally, we construct a BBA m_1 using the above distances to model the uncertainty of whether the center pixel is corrupted by the impulse noise or not according to the extreme criterion:

$$\begin{cases} m_1(N) = \dfrac{d_c - d_0}{d_{\text{ext}} - d_0 + \varepsilon} \\ m_1(S) = 1 - \dfrac{d_c - d_{\text{med}}}{d_{\text{ext}} - d_{\text{med}}} \\ m_1(\Theta) = 1 - m_1(N) - m_1(S) \end{cases} \tag{10}$$

Here, the FOD $\Theta = \{N, S\}$, where N denotes the noise and S denotes the signal. The parameter ε is a small positive real number to avoid $m_1(N)$ to be 1, when the intensity of the center pixel is an extreme value. It means that a pixel with an extreme value should not be absolutely recognized as the noise because it might be the signal actually. Furthermore, Dempster's rule of combination in (5) has the problem of one ballot veto when one BBA is assigned 1 on one singleton θ_i ($\theta_i \in \Theta$), while 0 on other singletons. That is, if $m_1(N) = 1$, i.e., $m_1(S) = 0$, no matter what m_2 is, the combined BBA has $m(S) = 0$, which indicates the center pixel cannot be the signal.

Since $d_{\text{ext}} \geq d_c \geq d_0 \geq d_{\text{med}}$, $0 \leq (d_c - d_0)/(d_{\text{ext}} - d_0 + \varepsilon) < 1$ and $0 \leq (d_c - d_{\text{med}})/(d_{\text{ext}} - d_{\text{med}}) \leq 1$. That is, $0 \leq m_1(N) < 1$ and $0 \leq m_1(S) \leq 1$. Besides, as $d_{\text{med}} \leq d_0$,

$$m_1(N) \leq \frac{d_c - d_0}{d_{\text{ext}} - d_0} \leq \frac{d_c - d_{\text{med}}}{d_{\text{ext}} - d_{\text{med}}},$$

which means $m_1(N) \leq 1 - m_1(S)$ so that $m_1(N) + m_1(S) \leq 1$. Therefore, m_1 satisfies the constraint in (2), and m_1 is a legitimate BBA.

According to m_1, the center pixel will have a large value of $m_1(N)$ only when its intensity is close to the extreme value, and at the same time far from the intensity being the closest to the median of $\tilde{I}$ in W_D. The center pixel will have a large value of $m_1(S)$ when its intensity is close to the median of $\tilde{I}$.

Here, we consider two different cases about the detection window and the corresponding BBA m_1 of the center pixel when $\tilde{I} = [0, 255]$, $\varepsilon = 0.1$ and $\alpha = 10$, i.e., noise pixels take values in the sets of $S_1 = \{0, 1, \ldots, 10\}$ and $S_2 = \{245, 246, \ldots, 255\}$.

(a) For the most common case, the intensities of signal pixels in a detection window W_D are far from the extreme values, as the example shown in Fig. 4(a), where the intensity range of signal pixels is [100, 150]. The pixel with the intensity of 127 is the most unlikely to be the noise in W_D, since 127 is the farthest intensity in W_D from the extreme values. If the center pixel's intensity $x_{i,j}$ is in the range of [0, 10] or [245, 255], it is close to the extreme value, and at the same time far from 127. Thus, the center pixel is assigned a large value of $m_1(N)$. If the center pixel's intensity is in the range of [100, 150], it is close to the median of $\tilde{I}$. Thus, it is assigned a large value of $m_1(S)$.
(b) In some cases, all of the signal pixels' intensities in a detection window are close to an extreme value, as the example shown in Fig. 5(a), where the intensity range of signal pixels is [230, 250]. The pixel with the intensity of 230 is the one that is most unlikely to be the noise in W_D, since 230 is the farthest intensity in W_D from the extreme values. If the center pixel's intensity $x_{i,j}$ is in the range of [0, 10] or [241, 255], it is close to the extreme value and far from 230. Thus, the center pixel is assigned a large value of $m_1(N)$. If the center pixel's intensity $x_{i,j}$ is in the range of [230, 240], the center pixel is assigned a small value of $m_1(N)$ since its intensity is close to 230. At the same time, it is assigned a small value of $m_1(S)$ since $x_{i,j}$ is far from the median of $\tilde{I}$. Therefore, $m_1(\Theta)$ is large, which indicates it is hard to say whether the center pixel is the noise or signal.
In summary, in this case, it is hard to get a crisp description of the beliefs for the corresponding decisions according to the extreme criterion, since the intensity range of signal pixels overlaps with that of the noise pixels. However, our BBA m_1 keeps the large uncertainty (large $m_1(\Theta)$), which is helpful to avoid the arbitrary detection decision.

From the above we can see that when using the extreme criterion for noise detection, our evidential method uses the BBA to de-

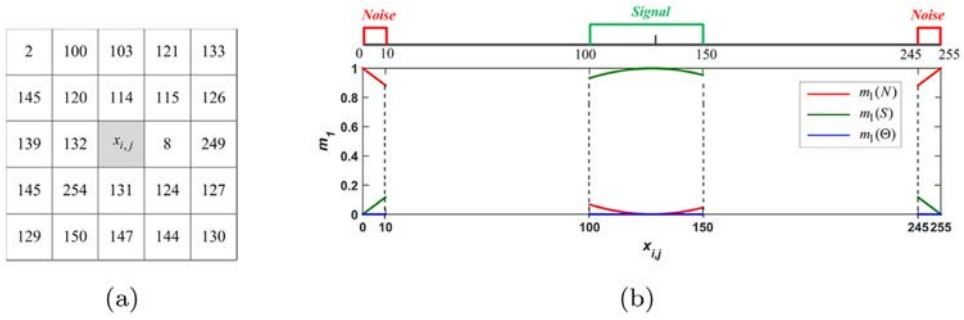

Fig. 4. Case *a* and the corresponding m_1 of the center pixel. (a) A detection window for case *a*. (b) Corresponding m_1 when x takes different values.

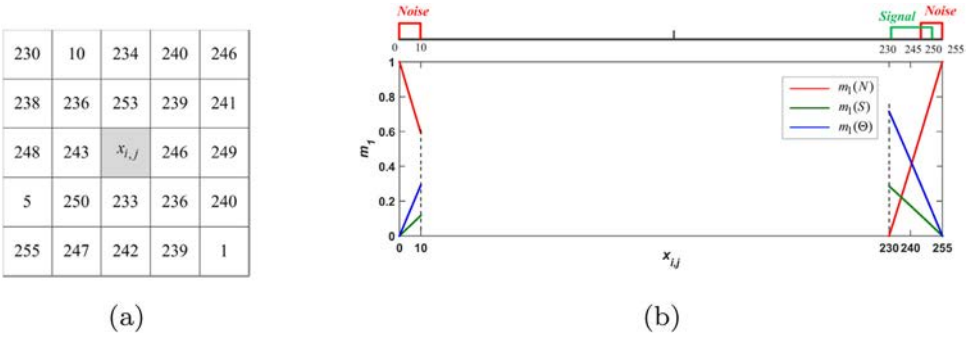

Fig. 5. Case *b* and the corresponding m_1 of the center pixel. (a) A detection window for case *b*. (b) Corresponding m_1 when x takes different values.

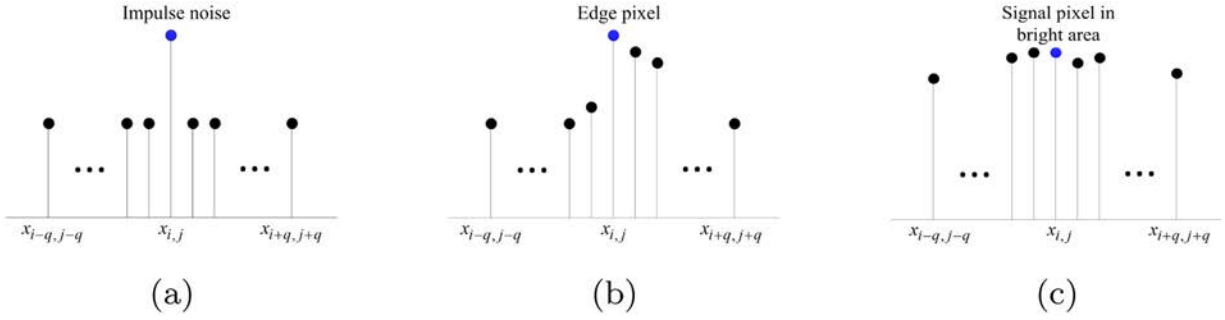

Fig. 6. One-dimensional illustration of the differences between some signal pixels and the impulse noise. (a) Intensities of the impulse noise and its neighbors. (b) Intensities of an edge pixel and its neighbors. (c) Intensities of signal pixels in the bright area.

scribe the beliefs of the corresponding detection decisions, which does not make a hard decision like two-steps methods but keeps the uncertainty. This is more cautious and can reduce the information loss for the final fusion-based detection.

2) *Evidential modeling for the uncertainty in discontinuity criterion* According to the discontinuity property of the impulse noise, the intensity of an impulse noise pixel tends to be much higher or lower than the intensities of its neighbors. For some signal pixels, e.g., edge pixels and signal pixels in the bright or dark area, they are easily detected as the noise according to the extreme criterion. However, they have some differences from the noise pixel according to the discontinuity criterion. The intensity of an edge pixel is higher or lower than only a portion of the intensities of its neighbors. The intensity of a signal pixel in the bright or dark area is similar to the intensities of its neighbors.

For a pixel at (i, j), we consider its neighbors' intensity information in the same detection window $W_D(i, j) = \{x_{i-s,j-t} | -(w_D - 1)/2 \le s, t \le (w_D - 1)/2\}$ as used in modeling the uncertainty in the extreme criterion. Those differences between the signal, edge, and the bright area pixels reflected in the discontinuity property are illustrated in Fig. 6. Here for simplification, one-dimensional expressions of the pixels' intensities in the detection windows are used, where $q = (w_D - 1)/2$.

We use the rank-ordered absolute differences (ROAD) statistic [29] to describe such differences reflected in the discontinuity property. Define $dif(x_{i,j}, x_{i-s,j-t}) = x_{i,j} - x_{i-s,j-t}$ as the absolute difference of the intensities between the center pixel at (i, j) and its neighbor at $(i - s, j - t)$, where $x_{i-s,j-t} \in W_D(i, j)$. If the size of $W_D(i, j)$ is $M = w_D \times w_D$, there will be $M - 1$ neighbors in the window, and therefore the amount of $dif(x_{i,j}, \cdot)$ is $M - 1$. These $dif(x_{i,j}, \cdot)$ can describe the dissimilarity between the center pixel and its neighbors. To further analyze this dissimilarity, sort these $M - 1$ $dif(x_{i,j}, \cdot)$ values in the ascending order and denote $r_g(x_{i,j})$ as the gth smallest $dif(x_{i,j}, \cdot)$. Finally, calculate the sum of the first n smallest $dif(x_{i,j}, \cdot)$ as

$$\mathrm{ROAD}_n(x_{i,j}) = \sum_{g=1}^{n} r_g(x_{i,j}) \tag{11}$$

where $2 \le n \le M - 1$.

If the center pixel is the noise, $dif(x_{i,j}, \cdot)$ is small when its neighbor is a noise pixel whose intensity is close to the same extreme value as the center pixel.

If the center pixel is the signal without extreme property, $dif(x_{i,j},\cdot)$ is large when its neighbor is the noise.

If the center pixel is the signal with extreme property, $dif(x_{i,j},\cdot)$ is large when its neighbor is a noise whose intensity is close to the other extreme value.

Therefore, when the noise density is low, the impulse noise has large value of $\mathrm{ROAD}_{M-1}(x_{i,j})$ as well as the sum of its smallest n $dif(x_{i,j},\cdot)$ values, i.e., $\mathrm{ROAD}_n(x_{i,j})$. The signal pixel has small value of $\mathrm{ROAD}_{M-1}(x_{i,j})$ as well as $\mathrm{ROAD}_n(x_{i,j})$.

With the increase of the noise density, the quantity of impulse noise pixels increases in a detection window. If the center pixel is the noise, the amount of small $dif(x_{i,j},\cdot)$ will increase since there are more noise neighbors having the similar intensities with the center pixel. At the same time, the amount of very large $dif(x_{i,j},\cdot)$ also increases since there are more noise neighbors having the intensities close to the other extreme value. Thus, $\mathrm{ROAD}_n(x_{i,j})$ becomes smaller but $\mathrm{ROAD}_{M-1}(x_{i,j})$ has no significant change.

If the center pixel is the signal, the amount of large $dif(x_{i,j},\cdot)$ will increase since there are more noise neighbors. Thus, $\mathrm{ROAD}_{M-1}(x_{i,j})$ becomes larger but $\mathrm{ROAD}_n(x_{i,j})$ has no significant change.

In summary, $\mathrm{ROAD}_n(x_{i,j})$ is large only when the center pixel is the noise and the noise density is small; $\mathrm{ROAD}_{M-1}(x_{i,j})$ is small only when the center pixel is the signal and the noise density is small. With the increasing of the noise density, the differences between the signal and the noise reflected in $\mathrm{ROAD}_n(x_{i,j})$ and $\mathrm{ROAD}_{M-1}(x_{i,j})$ narrow. This means that the discontinuity property of the impulse noise pixels becomes weaker with the increase of the noise density. It is unreasonable to use the discontinuity criterion to make hard decisions for detection. Therefore, we construct a BBA m_2 to describe the beliefs of the corresponding detection decisions according to the discontinuity criterion.

As we have discussed above, only the noise pixel can have large $\mathrm{ROAD}_n(x_{i,j})$ and only the signal pixel can have small $\mathrm{ROAD}_{M-1}(x_{i,j})$. Thus, for a given center pixel, the larger value of $\mathrm{ROAD}_n(x_{i,j})$ it has, the larger belief it should be assigned to being detected as the noise; the smaller value of $\mathrm{ROAD}_{M-1}(x_{i,j})$ it has, the larger belief should be assigned to being detected as the signal. For a center pixel with the intensity of $x_{i,j}$, its m_2 is constructed as follow. We take $n=(M-1)/2$, which means that we focus on the first half small $dif(x_{i,j},\cdot)$ when considering the belief of that a pixel should be detected as the noise.

$$\begin{cases} m_2(N) = \dfrac{\mathrm{ROAD}_{\frac{(M-1)}{2}}(x_{i,j})}{\frac{(M-1)}{2}\times(I_{\max}-I_{\min})} \\ m_2(S) = 1-\dfrac{\mathrm{ROAD}_{M-1}(x_{i,j})}{(M-1)\times(I_{\max}-I_{\min})} \\ m_2(\Theta) = 1-m_2(N)-m_2(S) \end{cases} \tag{12}$$

Here, $I_{\max}$ and $I_{\min}$ denote the maximum and minimum intensities of the whole image, respectively.

Since $r_g(x_{i,j}) \le I_{\max}-I_{\min}$, $\mathrm{ROAD}_{\frac{(M-1)}{2}}(x_{i,j}) \le \frac{(M-1)}{2}\times(I_{\max}-I_{\min})$ and $\mathrm{ROAD}_{M-1}(x_{i,j}) \le (M-1)\times(I_{\max}-I_{\min})$. That is $0\le m_2(N)\le 1$ and $0\le m_2(S)\le 1$. Besides, since

$$\begin{aligned} &m_2(N)+m_2(S) \\ &= 1-\left(\frac{\mathrm{ROAD}_{M-1}(x_{i,j})}{(M-1)\times(I_{\max}-I_{\min})}-\frac{\mathrm{ROAD}_{(M-1)/2}(x_{i,j})}{\frac{(M-1)}{2}\times(I_{\max}-I_{\min})}\right) \\ &= 1-\frac{\sum_{g=\frac{(M+1)}{2}}^{M-1} r_g(x_{i,j})-\mathrm{ROAD}_{(M-1)/2}(x_{i,j})}{(M-1)\times(I_{\max}-I_{\min})} \end{aligned}$$

and $\sum_{g=\frac{(M+1)}{2}}^{M-1} r_g(x_{i,j}) \ge \mathrm{ROAD}_{\frac{(M-1)}{2}}(x_{i,j})$, there exists $m_2(N)+m_2(S)\le 1$. Thus, m_2 satisfies the constraint of BBA in (2) and m_2 is a legitimate BBA.

For a given pixel, mass values in the BBA m_2: $m_2(N)$, $m_2(S)$ and $m_2(\Theta)$ can be represented as the areas of regions as shown in Fig. 7.

Fig. 7(a) illustrates an example of a detection window. The intensity of the center pixel $x_{i,j}=2$. We suppose that the largest intensity difference $I_{\max}-I_{\min}$ in the image is 255. Since the size of the window M is 25, we can get 24 $dif(x_{i,j},\cdot)$ values. The ascending ordered $dif(x_{i,j},\cdot)$, i.e., $r_g(x_{i,j})$, $(g=1,2,\ldots,24)$, are expressed as the histogram in Fig. 7(b). We specify the area of the rectangular region in Fig. 7(b) with the vertex points: (0, 0), (24, 0), (0, 255) and (24, 255) as 1. It means that we represent the value of $(M-1)\times(I_{\max}-I_{\min})$ in (12) using a region with an area of 1. Thus, the value of $\mathrm{ROAD}_{M-1}(x_{i,j})/[(M-1)\times(I_{\max}-I_{\min})]$ can be represented by the region determined by $r_g(x_{i,j})$, $(g=1,2,\ldots,24)$ in Fig. 7(b). That is, the value of $m_2(S)$ in (12), i.e., $1-\mathrm{ROAD}_{M-1}(x_{i,j})/[(M-1)\times(I_{\max}-I_{\min})]$ can be represented as the blue area in Fig. 7(c). Similarly, the value of $\mathrm{ROAD}_{(M-1)/2}(x_{i,j})/[(M-1)\times(I_{\max}-I_{\min})]$ can be represented by the region determined by $r_g(x_{i,j})$, $(g=1,2,\ldots,12)$ in Fig. 7(b). That is, the value of $m_2(N)$ in (12), i.e., $2\times\mathrm{ROAD}_{(M-1)/2}(x_{i,j})/[(M-1)\times(I_{\max}-I_{\min})]$, can be represented as the pink area[1] in Fig. 7(c). Thus, the value of $m_2(\Theta)$ is represented as the remanent area, i.e. the green area in Fig. 7(c).

Fig. 8 shows the graphical representations of m_2 for different kinds of center pixels with different noise density levels (25%, 50% and 75%). Center pixels include the impulse noise pixel (the first column in Fig. 8), the signal pixels with extreme property, such as the edge pixel (the second column in Fig. 8), the signal pixels in the bright or dark area (the third column in Fig. 8), and the common signal pixels with no extreme property (the last column in Fig. 8). Here, we assume that the largest intensity differences $I_{\max}-I_{\min}$ for the whole image in all cases are 255.

In Fig. 8, the signal pixels (from the second column to the last column) have large values of $m_2(S)$ indicating that for signal pixels, large beliefs are assigned to being detected as the signal under all noise density levels.

For the impulse noise pixel, when the noise density $\le$ 50% (Fig. 8(a) or (e)), it has large value of $m_2(N)$ indicating that large belief is assigned to being detected as the noise. However, when the noise density is larger than 50% (Fig. 8(i)), the impulse noise pixel has small value of $m_2(N)$ indicating that only small belief is assigned to being detected as the noise. But at the same time, its value of $m_2(\Theta)$ is large indicating that the uncertainty degree of discontinuity criterion is large when the image is corrupted severely.

Our evidential method uses the BBA to describe the beliefs of the corresponding detection decisions according to the discontinuity criterion. We do not make the hard decision directly but keep the uncertainty for the time being, which is more cautious. Particularly, our modeling method here keeps the large uncertainty of discontinuity criterion when the noise intensity is large. This will be helpful for the final fusion-based detection to decrease the miss-detections and false alarms.

3) *Fusion based detection* The generated BBAs m_1 and m_2 can be combined, e.g., using Eq. (5) to obtain $m(\cdot)=[m_1\oplus m_2](\cdot)$, which is a combined BBA for the noise detection representing the simultaneous use of the extreme property and discontinuity property. Once m is obtained, we use the pignistic probability transformation in Eq. (6) to transform m into a probability measure BetP. If $\mathrm{BetP}(N)\ge 0.5$, the center pixel should be detected as the noise.

[1] Since the value of $m_2(N)$ is the double of $\mathrm{ROAD}_{(M-1)/2}(x_{i,j})/[(M-1)\times(I_{\max}-I_{\min})]$, $m_2(N)$ can be represented as the double of the region determined by $r_g(x_{i,j})$, $(g=1,2,\ldots,12)$.

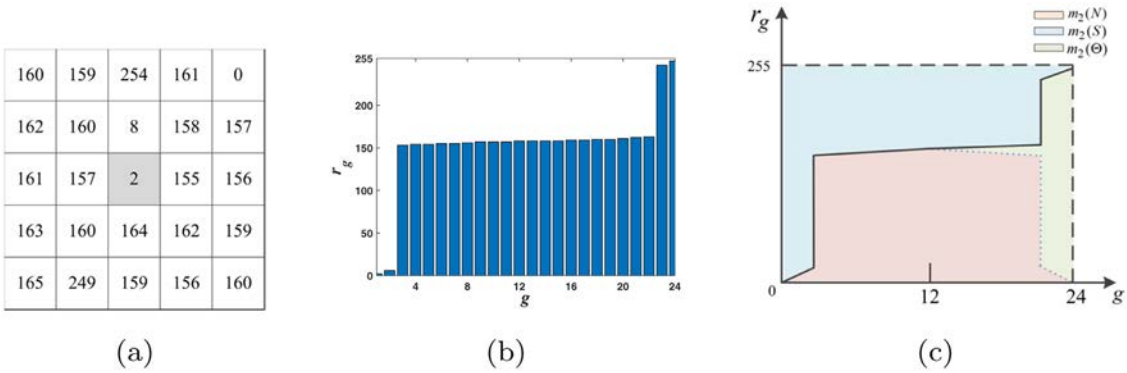

Fig. 7. Visual representation of m_2. (a) A detection window. (b) The illustration of $r_g(2)$. (c) Graphical representation of belief assignments. (For interpretation of the references to colour in this figure legend, the reader is referred to the web version of this article.)

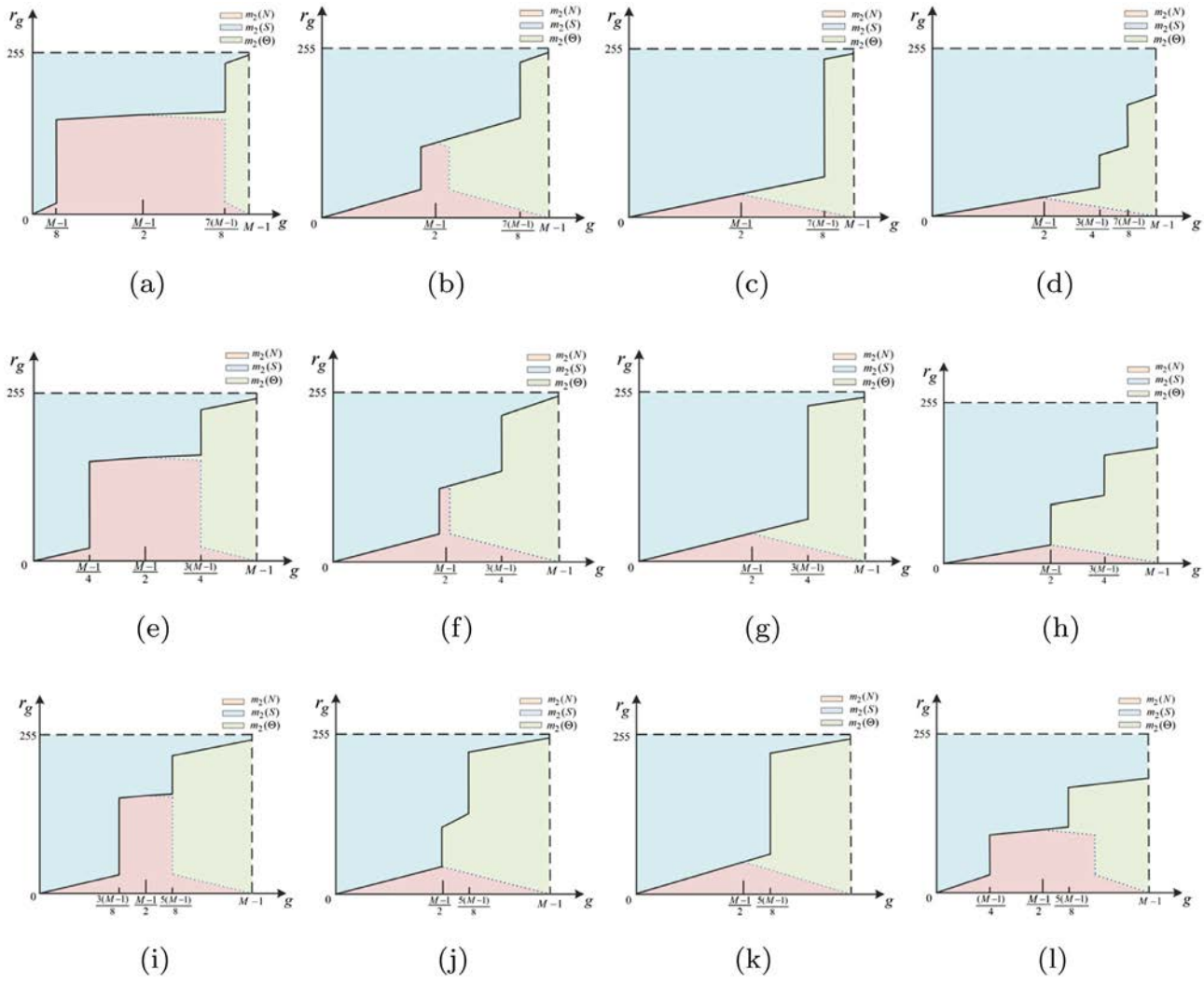

Fig. 8. Illustration of m_2 in cases with different noise densities. (From top to bottom, from left to right) The first row to third row show the cases when the noise densities are 25%, 50% and 75% respectively. The first column to fourth column show the cases when the center pixels are the impulse noise, edge pixel, signal pixel in the bright or dark area and common signal pixel without extreme property respectively.

Here we use an example to illustrate our detection procedure. A detection window is shown in Fig. 9.

In this window, intensities of signal pixels range from 200 to 206 and several pixels are corrupted by the impulse noise with intensities of 0, 8 or 9. Assume the intensity range of the whole image is [0, 255]. The value of ε in (10) is 0.1.

According to the modeling method I, the generated BBAs are:

$$\begin{cases} m_1(N) = 0.8416 \\ m_1(S) = 0.0933 \\ m_1(\Theta) = 0.0651 \end{cases} \quad \text{and} \quad \begin{cases} m_2(N) = 0.5696 \\ m_2(S) = 0.3320 \\ m_2(\Theta) = 0.0984 \end{cases}$$

202	203	203	201	206
201	202	8	204	204
203	200	8	0	202
200	9	201	204	204
200	201	200	204	202

Fig. 9. The illustration of a detection window.

The combined BBA is:

$$\begin{cases} m(N) = 0.8978 \\ m(S) = 0.0926 \\ m(\Theta) = 0.0096 \end{cases}$$

Then, we obtain the pignistic probability $\mathrm{BetP}(N) = 0.9026$ and the center pixel is finally detected as the impulse noise since $\mathrm{BetP}(N) > 0.5$.

3.2.2. Evidential modeling method II and fusion based detection

The impulse noise detection with two criteria including the extreme property and discontinuity property can be viewed as a multi-criteria (to be more accurately bi-criteria) decision making problem. Therefore, we can use the cautious ordered weighted averaging with evidential reasoning (COWA-ER) method [34] to generate BBAs and to implement the fusion-based noise detection.

1) *COWA-ER method*: In the noise detection problem, for a given pixel, the finite set of alternatives $\Theta = \{\theta_1, \theta_2\} = \{N, S\}$. According to the analyses in method I, the pessimistic and optimistic valuations of the expected payoffs to these alternatives obtained from the two detection criteria (extreme criterion and discontinuity criterion) are:

$$\begin{cases} e_{\min}(N) = \min\left\{ \dfrac{d_c - d_0}{d_{\text{ext}} - d_0 + \varepsilon}, \dfrac{\mathrm{ROAD}_{\frac{M-1}{2}}(x_{i,j})}{\frac{M-1}{2} \times (I_{\max} - I_{\min})} \right\} \\ e_{\max}(N) = \max\left\{ \dfrac{d_c - d_0}{d_{\text{ext}} - d_0 + \varepsilon}, \dfrac{\mathrm{ROAD}_{\frac{M-1}{2}}(x_{i,j})}{\frac{M-1}{2} \times (I_{\max} - I_{\min})} \right\} \\ e_{\min}(S) = \min\left\{ 1 - \dfrac{d_c - d_{\text{med}}}{d_{\text{ext}} - d_{\text{med}}}, 1 - \dfrac{\mathrm{ROAD}_{M-1}(x_{i,j})}{(M-1) \times (I_{\max} - I_{\min})} \right\} \\ e_{\max}(S) = \max\left\{ 1 - \dfrac{d_c - d_{\text{med}}}{d_{\text{ext}} - d_{\text{med}}}, 1 - \dfrac{\mathrm{ROAD}_{M-1}(x_{i,j})}{(M-1) \times (I_{\max} - I_{\min})} \right\} \end{cases} \tag{13}$$

Then, the expected payoff matrix is constructed as:

$$E = \begin{bmatrix} E[N] \\ E[S] \end{bmatrix} = \begin{bmatrix} [e_{\min}(N), e_{\max}(N)] \\ [e_{\min}(S), e_{\max}(S)] \end{bmatrix} \tag{14}$$

Here, the expected payoffs $E[N]$ and $E[S]$ are imprecise since they belong to the interval $[e_{\min}(\cdot), e_{\max}(\cdot)]$ where the lower and upper bounds represent the pessimistic and optimistic attitudes, respectively.

Then, divide each bound of intervals by the max of the bounds, i.e., $e_{\mathrm{MAX}} = \max\{e_{\max}(N), e_{\max}(S)\}$, to get a new normalized imprecise expected payoff vector E^{Imp}:

$$E^{\mathrm{Imp}} = \begin{bmatrix} [e_{\min}(N)/e_{\mathrm{MAX}}, e_{\max}(N)/e_{\mathrm{MAX}}] \\ [e_{\min}(S)/e_{\mathrm{MAX}}, e_{\max}(S)/e_{\mathrm{MAX}}] \end{bmatrix} = \begin{bmatrix} [a_1, b_1] \\ [a_2, b_2] \end{bmatrix} \tag{15}$$

In the final, convert the normalized imprecise expected payoff vector E^{Imp} into BBAs according to a very natural and simple transformation [34,36]. The generation of a BBA associated to the hypothesis θ_i, $(\theta_1 = N, \theta_2 = S)$ from any imprecise value $[a_i, b_i] \subseteq [0, 1]$ is generated as:

$$\begin{cases} m_i(\theta_i) = a_i \\ m_i(\bar{\theta}_i) = 1 - b_i \\ m_i(\theta_i \cup \bar{\theta}_i) = b_i - a_i \end{cases} \tag{16}$$

$\bar{\theta}_i$ is the complement of θ_i in Θ. With such a conversion, one sees that $Bel(\theta_i) = a_i$, $Pl(\theta_i) = b_i$ and the uncertainty is represented by the length of the interval $[a_i, b_i]$.

2) *Fusion based detection*: By using the COWA-ER method, we can obtain two BBAs: m_1 and m_2. The generated BBAs can be combined using Eq. (5), that is $m(\cdot) = [m_1 \oplus m_2](\cdot)$. Once m is computed, we use the pignistic probability transformation in (6) to transform m into a probability measure BetP. If $\mathrm{BetP}(N) \geq 0.5$, the center pixel should be detected as the impulse noise.

Here we consider the same example showed in Fig. 9. The value of ε in Eq. (13) is 0.1. The BBAs generated from modeling method II are:

$$\begin{cases} m_1(N) = 0.6768 \\ m_1(S) = 0 \\ m_1(\Theta) = 0.3232 \end{cases} \quad \text{and} \quad \begin{cases} m_2(N) = 0.6055 \\ m_2(S) = 0.1109 \\ m_2(\Theta) = 0.2836 \end{cases}$$

The combined BBA is:

$$\begin{cases} m(N) = 0.8622 \\ m(S) = 0.0388 \\ m(\Theta) = 0.0990 \end{cases}$$

Then, we get the pignistic probability $\mathrm{BetP}(N) = 0.9117$ and the center pixel is finally detected as the impulse noise because $\mathrm{BetP}(N) > 0.5$.

When modeling the uncertainty of noise detection, the two proposed methods use the same information (extreme criterion and discontinuity criterion) but generate belief functions in different ways. Either of these two methods can be an alternative to the other in many cases but they might generate different detection results in some special situations.

3.2.3. Different detection results with contradictory evidences

In many cases, the two proposed methods generate same detection results since they describe the extreme criterion and discontinuity criterion in very similar ways and both of their combined evidences will assign a larger belief to the same candidate (noise or signal). However, when these two evidence sources are highly contradictory (extreme criterion and discontinuity criterion give very different supports to the target pixel), the two proposed methods might generate different detection results as illustrated in the following two different examples that the evidence sources are highly contradictory.

1) *Detection results for situation 1*

Situation 1 describes the situation when the target pixel is a signal in a dark area close to an edge where the pixels at the other side of the edge have higher intensities as shown in Fig. 10.

According to the extreme criterion and discontinuity criterion, the two BBAs generated by evidential modeling method I using Eqs. (10) and (12) are:

$$\begin{cases} m_1(N) = 0.9548 \\ m_1(S) = 0.0235 \\ m_1(\Theta) = 0.0217 \end{cases} \quad \text{and} \quad \begin{cases} m_2(N) = 0.0039 \\ m_2(S) = 0.9440 \\ m_2(\Theta) = 0.0521 \end{cases}$$

1	1	2	2	1
0	0	0	1	2
9	3	2	3	4
50	41	28	18	15
26	34	44	45	41

Fig. 10. Highly contradictory situation 1.

249	223	252	7	7
220	219	248	249	253
6	252	246	0	9
254	246	2	209	245
219	219	251	245	247

Fig. 11. Highly contradictory situation 2. (For interpretation of the references to colour in this figure legend, the reader is referred to the web version of this article.)

In this situation, the proposition that the target pixel should be detected as noise obtained very different supports from the extreme criterion ($m_1(N)$ is large) and discontinuity criterion ($m_2(N)$ is small) since the target pixel's intensity is very close to the extreme value 0, but at the same time, the target pixel has many neighborhoods have the similar intensities. After the evidence combination and probability transformation, we finally get $BetP(N) = 0.5491$ and the target pixel is false alarmed as noise since $BetP(N) > 0.5$.

The evidential modeling method II deals with these two highly contradictory evidences in different ways. According to Eqs. 13 and 14, the expected payoff matrix is generated as:

$$E = \begin{bmatrix} E[N] \\ E[S] \end{bmatrix} = \begin{bmatrix} [0.0039, 0.9548] \\ [0.0235, 0.9440] \end{bmatrix}$$

Then, we get the normalized expected payoff vector:

$$E^{\text{Imp}} = \begin{bmatrix} E[N] \\ E[S] \end{bmatrix} = \begin{bmatrix} [0.0041, 1.0000] \\ [0.0246, 0.9887] \end{bmatrix}$$

The generated BBAs are:

$$\begin{cases} m_1(N) = 0.0041 \\ m_1(S) = 0 \\ m_1(\Theta) = 0.9959 \end{cases} \text{and} \quad \begin{cases} m_2(N) = 0.0113 \\ m_2(S) = 0.0246 \\ m_2(\Theta) = 0.9641 \end{cases}$$

After the evidence combination and probability transformation, we finally get $BetP(N) = 0.4954$ and the target pixel is successfully detected as signal since $BetP(N) < 0.5$. For this example, the detection result generated by the proposed method II is more reasonable.

2) *Detection results for situation 2*

Situation 2 describes the highly corrupted situation when the target pixel is noise and the neighborhood signal pixels (colored with green) have similar intensities with the target pixel as shown in Fig. 11.

According to Eqs. (10) and (12), the two BBAs generated by evidential modeling method I are:

$$\begin{cases} m_1(N) = 0.7914 \\ m_1(S) = 0.1049 \\ m_1(\Theta) = 0.1037 \end{cases} \text{and} \quad \begin{cases} m_2(N) = 0.0141 \\ m_2(S) = 0.7296 \\ m_2(\Theta) = 0.2564 \end{cases}$$

In this situation, the proposition that the target pixel should be detected as noise obtained very different supports from the extreme criterion ($m_1(N)$ is large) and discontinuity criterion ($m_2(N)$ is small) since the target pixel's intensity is close to the extreme value 255, but at the same time, there are many neighborhoods have the similar intensities with the target pixel. After the evidence combination and probability transformation, we finally get $BetP(N) = 0.5432$ and the target pixel is successfully detected as noise since $BetP(N) > 0.5$.

The evidential modeling method II deals with these two highly contradictory evidences in different ways. According to Eqs. (13) and (14), the expected payoff matrix is generated as:

$$E = \begin{bmatrix} E[N] \\ E[S] \end{bmatrix} = \begin{bmatrix} [0.0141, 0.7914] \\ [0.1049, 0.7296] \end{bmatrix}$$

Then, we get the normalized expected payoff vector:

$$E^{\text{Imp}} = \begin{bmatrix} E[N] \\ E[S] \end{bmatrix} = \begin{bmatrix} [0.0178, 1.0000] \\ [0.1325, 0.9219] \end{bmatrix}$$

The generated BBAs are:

$$\begin{cases} m_1(N) = 0.0178 \\ m_1(S) = 0 \\ m_1(\Theta) = 0.9822 \end{cases} \text{and} \quad \begin{cases} m_2(N) = 0.0781 \\ m_2(S) = 0.1325 \\ m_2(\Theta) = 0.7894 \end{cases}$$

After the evidence combination and probability transformation, we finally get $BetP(N) = 0.4809$ and the target pixel is missdetected as signal since $BetP(N) < 0.5$. For this example, the detection result generated by the proposed method I is more reasonable.

From the above, the two proposed methods are likely to generate different detection results in highly contradictory situations.

4. Adaptive median filtering

After the noise detection, we focus on the filter implementation. It should be better that only the corrupted pixels will undergo the filtering. The size of the filtering window influences the filtering performance a lot, and the optimal window size is usually determined by the detection result. Therefore, in this paper we further propose an adaptive switch median filtering method, which adaptively determines the size of filtering window according to the detection result.

For a given pixel at (i, j), the filtering window with a size of $w_F \times w_F$ centered at it is:

$$W_F(i, j) = \{x_{i-s,j-t} | -(w_F - 1)/2 \le s, t \le (w_F - 1)/2\} \tag{17}$$

where $x_{i-s,j-t}$ is the intensity of the pixel at $(i - s, j - t)$.

Generally, in order to preserve details better, the size of filtering window should be as small as possible if there are enough signal pixels in the filtering window to help determine the filtered value. In the current filtering window $W_F(i, j)$, the proportion of the detected signal pixels is:

$$S_{\text{pro}}^{W_F} = \frac{S_{\text{num}}^{W_F}}{w_F \times w_F} \tag{18}$$

where $S_{\text{num}}^{W_F}$ is the number of the detected signal pixels in $W_F(i, j)$. If the proportion of signal pixels in the current filtering window, i.e., $S_{\text{pro}}^{W_F}$ is small, the size of the filtering window should be expanded to see if the proportion is large enough in a larger filtering window.

Table 1
Estimation results of noise density (%).

Actual	10	20	30	40	50	60	70	80	90
Method I	10.01	19.98	29.99	40.00	50.01	60.01	70.00	80.01	90.01
Method II	10.01	19.98	29.98	39.99	49.99	59.99	70.00	80.00	90.00

When the noise density is large, $S_{\text{pro}}^{W_F}$ is likely to be small. Thus, the minimum $S_{\text{pro}}^{W_F}$ required for not extending the filtering window size should be reduced with the increase of the noise density to avoid over smoothing. Therefore, the noise density should be estimated first.

4.1. Noise density estimation

The noise density is estimated according to the noise detection result:

$$\hat{d}_N = \frac{N_{\text{num}}}{P_{\text{num}}}. \tag{19}$$

Here, N_{num} is the total number of the detected noise pixels and P_{num} is the total number of the pixels in the image.

The performance of noise density estimation for corrupted Lena images are presented in Table 1, where method I and method II represent the two proposed evidential modeling methods respectively. In this experiment, noise pixels take values in the sets of $S_1 = \{0, 1, \ldots, 10\}$ and $S_2 = \{245, 246, \ldots, 255\}$, i.e., $\alpha = 10$. The values of ε in Eqs. (10) and (13) are 0.1. The size of W_D is 11×11 based on a great deal of tests. According to Table 1, the estimation results are very close to the actual noise densities indicating that our detection methods are effective, and they can be used to determine the size of filtering window.

4.2. Filtering method

According to the estimated noise density $\hat{d}_N$ and the proportion of the detected signal pixels $S_{\text{pro}}^{W_F}$, the condition of judging whether the current filtering window should be expanded or not, is set as:

$$S_{\text{pro}}^{W_F} > (1 - \hat{d}_N) \times \beta \tag{20}$$

Here, β is a scale factor taking value in the range of (0, 1). We set it as 1/4 based on a great deal of tests on various images. When the noise density is small, the minimum required $S_{\text{pro}}^{W_F}$ for not expanding the current filtering window is large; when the noise density is large, the minimum required $S_{\text{pro}}^{W_F}$ is small.

Our filtering method can be outlined below:

Step (1) Set the initial size of filtering window $w_F \times w_F$ to 3×3 and set the maximum window size to $w_F^{\max} \times w_F^{\max}$.

Step (2) Set a filtering window $W_F(i, j)$ centered at the target pixel at (i, j) with current size of $w_F \times w_F$.

Step (3) If the proportion of the detected signal pixels in the filtering window, i.e., $S_{\text{pro}}^{W_F}$ satisfies the criterion in Eq. (20), go to Step (5).

Step (4) Extend the filtering window size to $(w_F + 1) \times (w_F + 1)$ and repeat Steps (2) and (3) until the current filtering window size reaches $w_F^{\max} \times w_F^{\max}$.

Step (5) Apply a median filtering to the current filtering window. The output intensity $Y_{i,j} = \text{median}\{x_{i-s,j-t} | x_{i-s,j-t} \in W_F^D(S)\}$, where $W_F^D(S)$ is the set of all detected signal pixels in the current filtering window.

The maximum window size is empirically given in Table 2 based on a large quantities of tests on various images. In Table 2, different window sizes are suggested for different noise density levels.

Table 2
Recommended maximum size of filtering window.

Estimated noise density	$w_F^{\max} \times w_F^{\max}$
$0\% < \hat{d}_N \le 30\%$	3×3
$30\% < \hat{d}_N \le 50\%$	5×5
$50\% < \hat{d}_N \le 70\%$	7×7
$\hat{d}_N > 70\%$	9×9

5. Experiments

The adaptive switching median filtering method we proposed includes two components: the impulse noise detection and the adaptive filtering process. Since the noise detection plays a key role in the final denoising performance, we first evaluate the performance of the noise detection. Then, we evaluate the filtering performance of our proposed adaptively median filtering and the whole denoising performance of our proposed ASMF-DBER method, respectively. Furthermore, the computational cost and sensitivity of the parameters' setting of ASMF-DBER will be discussed. We will also check the adaptability of our ASMF-DBER for the value of α in the impulse noise model, which in fact controls the intensity range that the noise pixels take values in.

Experiments are carried out using several monochrome images (Fig. 12). The experiment results of several existing methods, i.e., BDND [18], IBDND [19], ACWM [20], ASWM [23], ROR-NLM [25] and WCSR [24] are also provided for comparison.

5.1. Performance evaluation of noise detection

For the two proposed noise detection methods (method I and method II) based on two different evidential modeling methods respectively, we evaluate their performances using corrupted Lena image and the results are shown in Table 3. The performances of ACWM, BDND, ASWM and ROR-NLM methods are also provided for comparison. The performance evaluation indices used here include the false alarm rate (FAR), miss-detection rate (MDR) and accuracy rate (AR):

$$\text{FAR} = \frac{FA_{\text{num}}}{S_{\text{num}}^{\text{A}}}, \tag{21}$$

$$\text{MDR} = \frac{MD_{\text{num}}}{N_{\text{num}}^{\text{A}}}, \tag{22}$$

$$\text{AR} = \frac{P_{\text{num}} - FA_{\text{num}} - MD_{\text{num}}}{P_{\text{num}}}. \tag{23}$$

Here, FA_{num} is the number of the actual signal pixels being detected as the noise, MD_{num} is the number of the actual noise pixels being detected as the signal, $S_{\text{num}}^{\text{A}}$ is the number of the actual signal pixels, $N_{\text{num}}^{\text{A}}$ is the number of the actual noise pixels, and P_{num} is the number of pixels in the image.

In this experiment, $\alpha = 10$, i.e., noise pixels take values in $S_1 = \{0, 1, \ldots, 10\}$ and $S_2 = \{245, 246, \ldots, 255\}$. Values of ε in Eqs. (10) and (13) are 0.1. The size of W_D is empirically determined as 11×11 based on a great deal of tests.

As shown in Table 3, when the noise density is no larger than 60%, the accuracy rates of these methods are all larger than 80%.

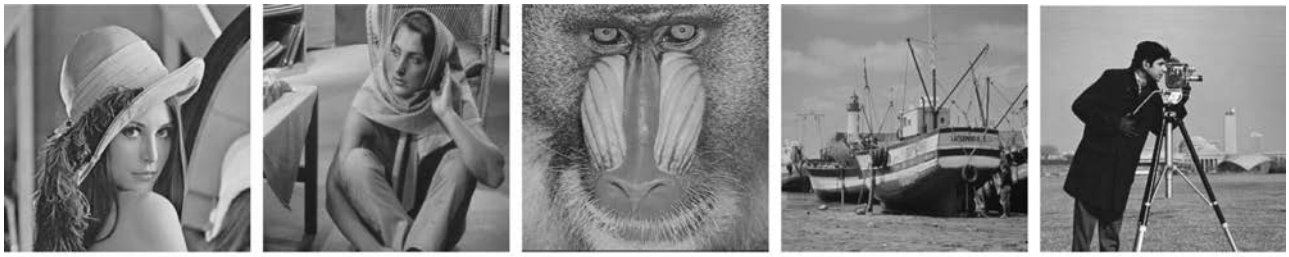

Fig. 12. Monochrome images for experiments. (a) Lena. (b) Barbara. (c) Baboon. (d) Boat. (e) Cameraman.

Table 3
Comparison of the noise detection performances for corrupted Lena images (%).

Noise density	Performance	ACWM	BDND	ASWM	ROR-NLM	Method I	Method II
10%	FAR	0.291	0.003	0.654	1.020	0.004	0.003
	MDR	0.302	0.023	0.317	0.019	0.237	0.191
	AR	99.708	**99.995**	99.380	99.080	99.973	99.978
20%	FAR	0.608	0.002	0.927	1.176	0.004	0.002
	MDR	0.967	0.264	0.485	0.086	0.116	0.122
	AR	99.320	99.946	99.161	99.042	**99.974**	**99.974**
30%	FAR	1.263	0.004	1.372	1.341	0.003	0.002
	MDR	2.995	1.123	0.855	0.157	0.046	0.107
	AR	98.217	99.660	98.783	99.014	**99.984**	99.967
40%	FAR	2.923	0.003	2.370	1.433	0.006	0.002
	MDR	6.975	2.941	1.924	0.414	0.004	0.042
	AR	95.456	98.822	97.808	98.975	**99.995**	99.982
50%	FAR	6.191	0.010	13.893	5.663	0.014	0.002
	MDR	12.864	6.057	3.492	1.634	0.003	0.027
	AR	90.473	96.967	91.308	96.351	**99.992**	99.986
60%	FAR	12.063	0.014	13.892	5.665	0.012	0.002
	MDR	20.921	10.387	11.785	6.513	0	0.005
	AR	82.622	93.762	87.372	93.826	99.995	**99.996**
70%	FAR	21.176	0.047	29.166	18.784	0.037	0.004
	MDR	30.789	15.587	22.981	18.742	0	0.002
	AR	72.095	89.075	75.164	81.245	99.989	**99.997**
80%	FAR	33.869	0.137	52.535	43.370	0.064	0.006
	MDR	41.782	21.976	36.742	35.514	0	0.001
	AR	59.801	82.392	60.099	62.915	99.987	**99.998**
90%	FAR	50.239	0.852	76.716	74.130	0.114	0.004
	MDR	52.852	29.431	38.678	48.875	0.001	0.001
	AR	47.409	73.427	57.518	48.600	99.988	**99.999**

When the noise density is larger than 60%, the accuracy rates of ACWM, BDND, ASWM and ROR-NLM methods drop rapidly. However, our proposed methods still achieve high accuracy rates ($\geq 90\%$).

5.2. Performance of filtering

To evaluate the filtering performance, we compare the filtering performance of the proposed adaptive median filtering method with the standard median filtering (SMF) used in ACWM, ASWM and the filters used in BDND, IBDND (adaptive weighted median filter), ROR-NLM and WCSR, respectively. In this experiment, $\alpha = 10$ and all the filters are used on the detected noise pixels generated by the proposed noise detection method I. The experimental result is shown in Fig. 13, where $F_{ROR-NLM}$, F_{BDND}, F_{IBDND} and F_{WCSR} denote the filters used in ROR-NLM, BDND, IBDND and WCSR algorithms respectively.

According to Fig. 13, when the noise density is no larger than 30%, the proposed filter has similar performance with the filters used in IBDND and WCSR. With the increase of the noise density, the proposed filter generates better performance than other filters.

5.3. Performance of denoising

To verify the whole denoising performance of our proposed ASMF-DBER, we compare the denoising performance of our proposed ASMF-DBER with ACWM, ASWM, ROR-NLM, BDND, IBDND and WCSR using PSNR and SSIM as shown in Figs. 14 and 15, respectively. In this experiment, $\alpha = 10$ and the size of detection window W_D is 11×11. ASMF-DBER I and II represent the denoising results based on the two proposed detection methods, respectively.

When the noise density is low ($\leq 20\%$), BDND, IBDND, and the proposed methods have similar denoising performances since they all can obtain high detection accuracy rates in low corrupted situations (as illustrated in Table 3 for Lena image) and have similar denoising performances when the noise detection results are accurate enough (as shown in Fig. 13 when only the actual noise pixels are filtered).

BDND and IBDND have better performance for Lena, Baboon and Boat images when the noise density is 10%. These images have no intensities close to extreme values (0 and 255). BDND and IBDND method can obtain better performance easily since they only uses extreme criterion when detecting impulse noise.

WCSR method has very good performance on Barbara image when the noise density is 10%. The reason is that Barbara im-

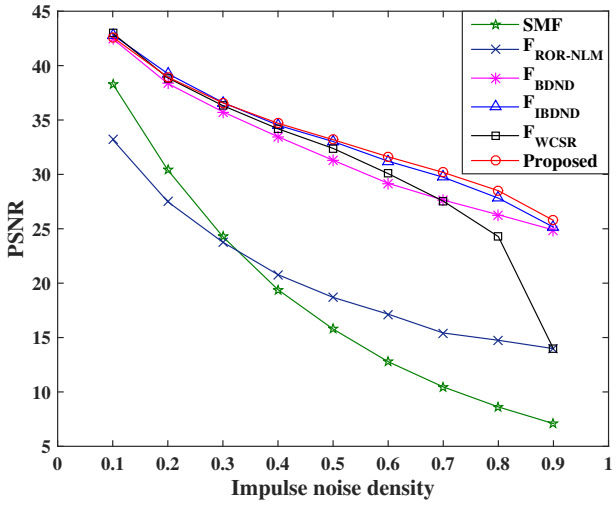

Fig. 13. Comparison of filtering performances using PSNR for corrupted Lena images.

age has big areas with regular texture. When the noise density is low, since the noise detection result is accurate enough, WCSR can reconstruct the texture very well using the trained dictionaries.

With the increase in noise density, the PSNR of BDND, IBDND and WCSR are much lower than that they achieved in Fig. 13 when only the actual noise pixels, but not the detected noise pixels, are filtered. That means, when carrying out the filtering on the detected impulse noise pixels, the detection result affects the whole denoising performance significantly. BDND, IBDND and WCSR fail to achieve satisfied filtering performances because of their poor detection results.

The subjective quality comparisons of filtered images are illustrated from Figs. 16–19. The false alarmed pixels and miss-detected pixels of the two proposed methods are colored with red and green, respectively. Except for Cameraman image, other test images do not have many false alarms and miss-detections. In order to highlight the colored pixels in these images, we circled the colored pixels using the corresponding colors (red for false alarms and green for miss-detections).

From the comparisons of quantitative results and visually subjective qualities, we can see that the proposed ASMF-DBER algorithms obtain superior denoising results compared with other switch median filters and the sparse representation based method. Particularly, in the high noise density cases, ASMF-DBER has obvious advantages over others.

For cameraman image, the pixels around the edge of the "cameraman" would obtain highly contradictory evidence supports from the extreme criterion and discontinuity criterion, as the highly contradictory situation 1 (Fig. 10), and the proposed two detection methods are likely to obtain different detection results. In Fig. 17, ASMF-DBER II has more false alarms than ASMF-DBER I at these pixels, so that the denoising performance of ASMF-DBER I for Cameraman image is not so good as ASMF-DBER II, as shown in Figs. 14(e) and 15(e).

Among these algorithms, WCSR has the most parameters (8 parameters) to be determined and some of them are sensitive with the noise density, what is a challenge for WCSR to obtain a satisfied denoising result.

From the above colored incorrect detections of the proposed two methods and Table 3, we can find that ASMF-DBER I gen-

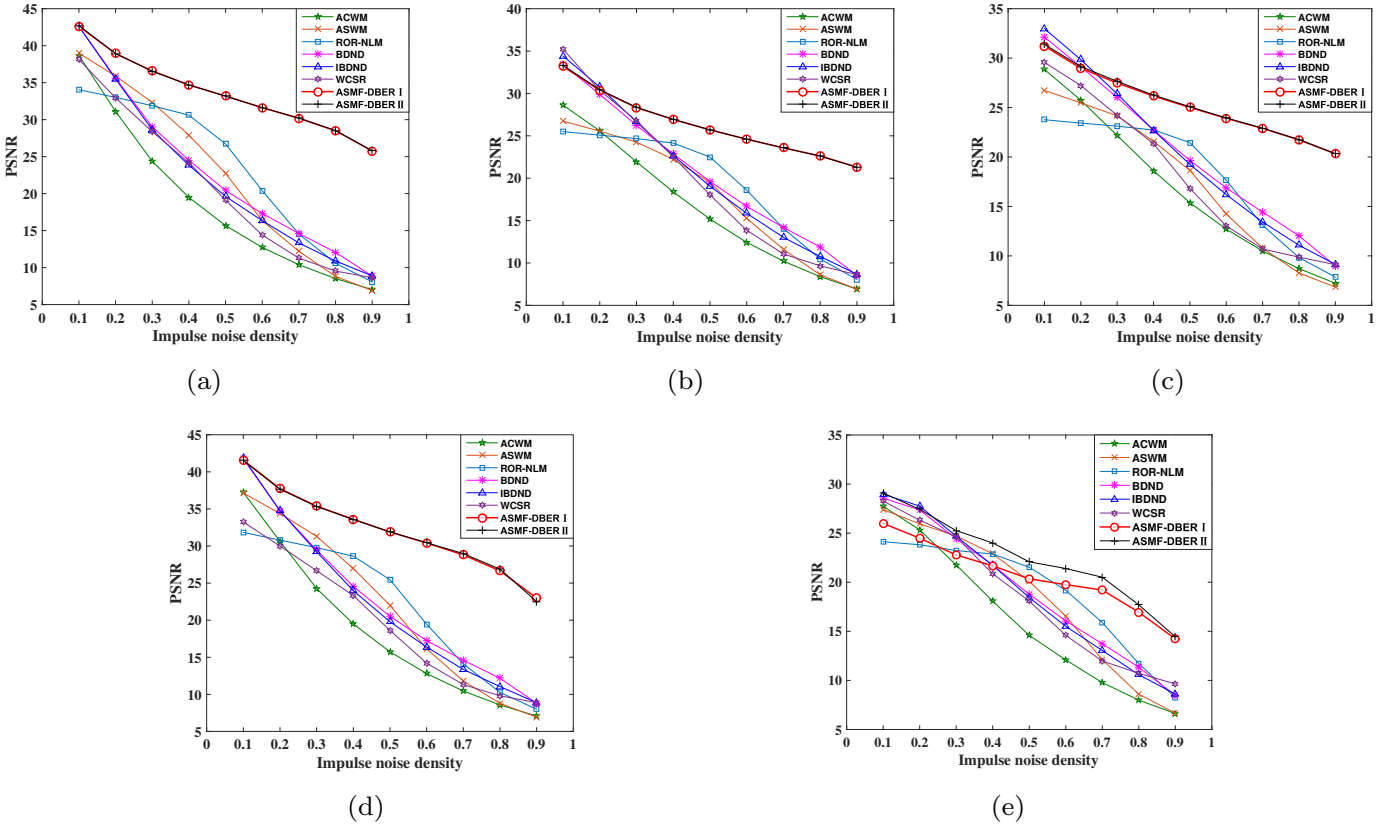

Fig. 14. Comparisons of denoising performances using PSNR. (a) Lena. (b) Barbara. (c) Baboon. (d) Boat. (e) Cameraman.

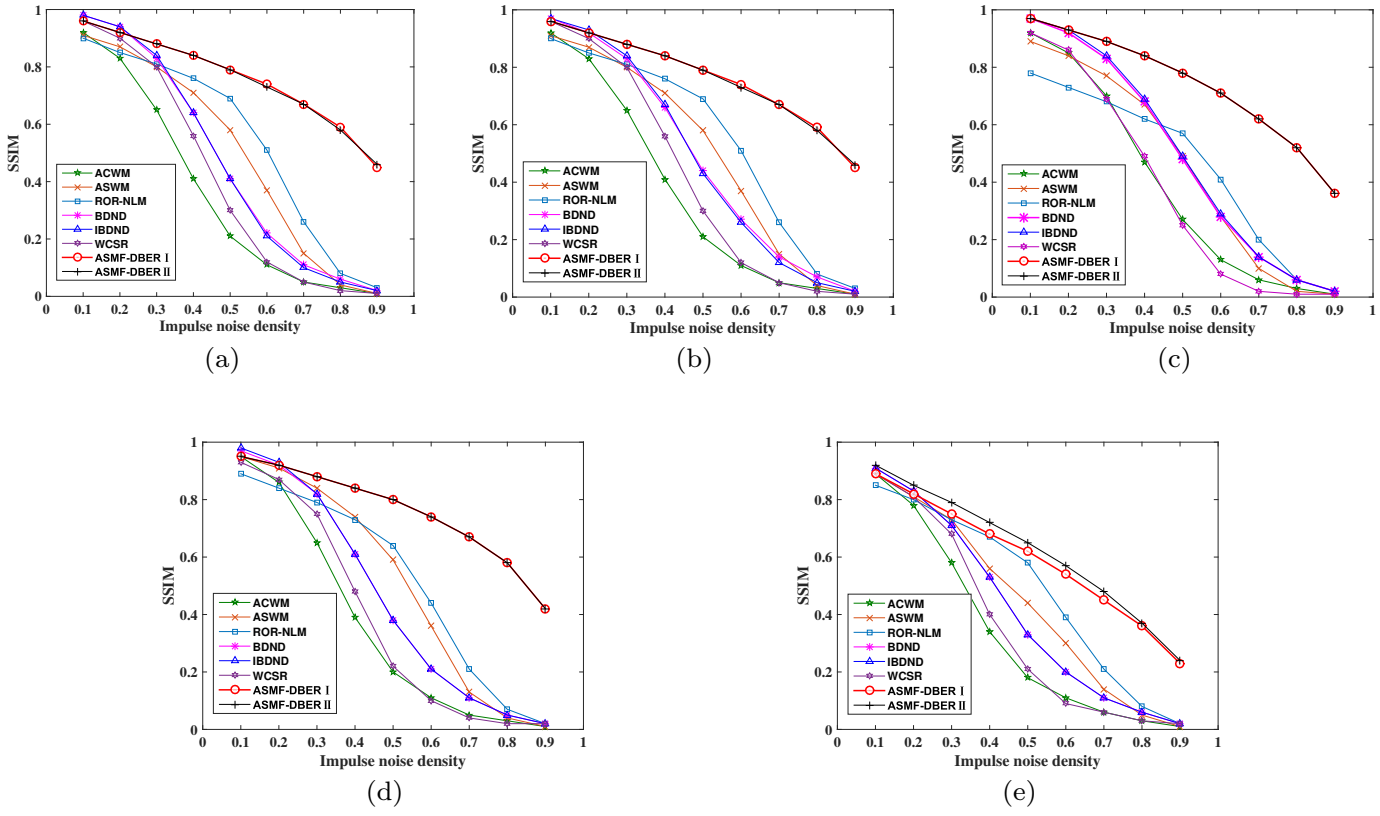

Fig. 15. Comparisons of denoising performances using SSIM. (a) Lena. (b) Barbara. (c) Baboon. (d) Boat. (e) Cameraman.

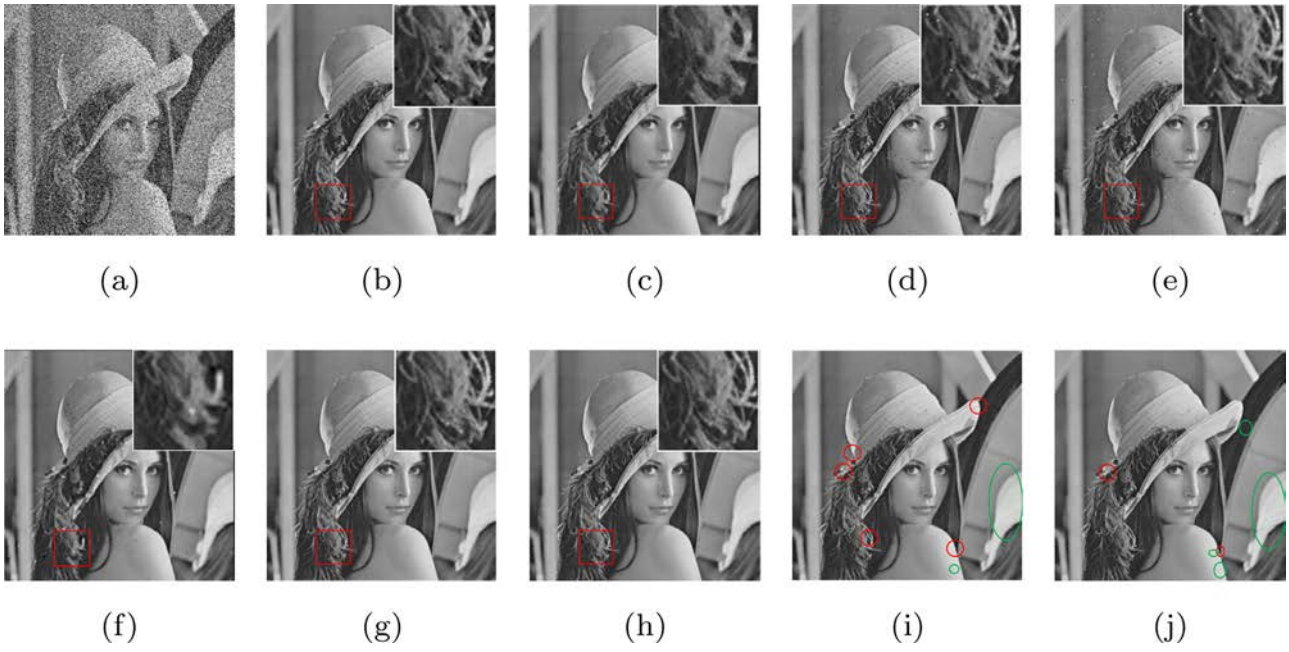

Fig. 16. Denoising results for Lena image (noise density is 30%). (a) Corrupted image. (b) ASWM. (c) ROR-NLM. (d) BDND. (e) IBDND. (f) WCSR. (g) ASMF-DBER I. (h) ASMF-DBER II. (i) Colored detection results of ASMF-DBER I. (j) Colored detection results of ASMF-DBER II. (For interpretation of the references to colour in this figure legend, the reader is referred to the web version of this article.)

erates more false alarms than ASMF-DBER II and ASMF-DBER II generates more miss-detections than ASMF-DBER I. Therefore, in practical applications, if the user relatively more emphasizes low miss-detection rate, we suggest ASMF-DBER I; if the user relatively more emphasizes low false-alarm rate, we suggest ASMF-DBER II.

5.4. Sensitivity of parameters' setting

There are two parameters to determine in our method. One is the detection window size and the other one is β in Eq. (20) used for deciding whether the current filtering window should be expanded or not. To discuss the sensitivity of the setting of these

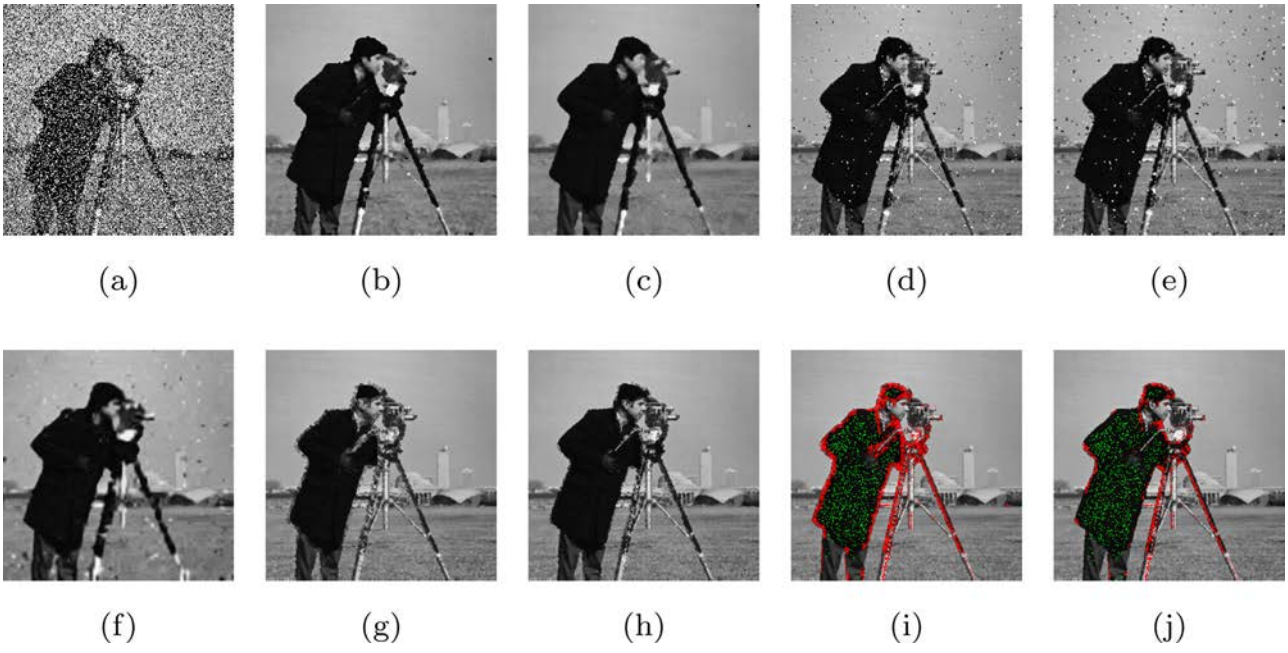

Fig. 17. Denoising results for Cameraman image (noise density is 40%). (a) Corrupted image. (b) ASWM. (c) ROR-NLM. (d) BDND. (e) IBDND. (f) WCSR. (g) ASMF-DBER I. (h) ASMF-DBER II. (i) Colored detection results of ASMF-DBER I. (j) Colored detection results of ASMF-DBER II. (For interpretation of the references to colour in this figure legend, the reader is referred to the web version of this article.)

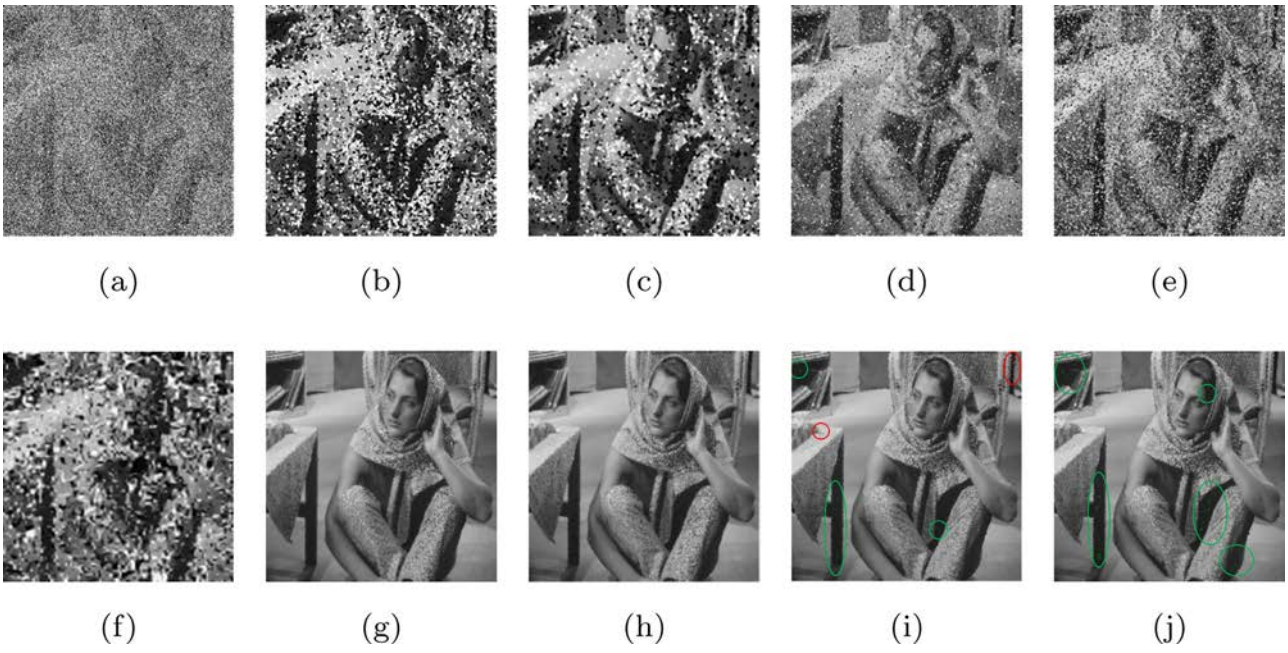

Fig. 18. Denoising results for Barbara image (noise density is 70%). (a) Corrupted image. (b) ASWM. (c) ROR-NLM. (d) BDND. (e) IBDND. (f) WCSR. (g) ASMF-DBER I. (h) ASMF-DBER II. (i) Colored detection results of ASMF-DBER I. (j) Colored detection results of ASMF-DBER II. (For interpretation of the references to colour in this figure legend, the reader is referred to the web version of this article.)

two parameters, we compare the denoising performances of all the combinations of the two parameters. The comparison results for the two proposed denoising methods are shown in Tables 4 and 5, respectively. In this experiment, β changes with an incremental step 1/8 from 1/8 to 7/8. The detection window size is set as 5×5, 7×7, 9×9, 11×11 or 13×13.

From Tables 4 and 5, the filtering performance is not very sensitive to the setting of β. When the noise density is 10% or 20%, all the β generate the same performance since the limited maximum filtering window is 3×3 when the estimated noise density is no larger than 30% according to Table 2. With the increase of the noise density, the denoising performance becomes poorer when selecting small size of detection window. When the noise density is higher than 70%, large detection windows (larger than 7×7) achieve obvious better denoising performance than small detection windows (no larger than 7×7). When the size of detection window is set as 11×11, and β is set as 1/4, we can usually obtain the best denoising performance.

Table 4
Denoising performances of ASMF-DBER I for different detection window size and β.

Noise	Density	10%	20%	30%	40%	50%	60%	70%	80%	90%
5×5	$\beta=1/8$	41.50	38.27	35.96	34.22	32.56	30.96	29.07	23.04	13.36
	$\beta=1/4$	41.50	38.27	35.96	34.26	32.59	30.96	29.09	23.07	13.36
	$\beta=3/8$	41.50	38.27	35.96	34.24	32.59	31.08	29.40	23.08	13.39
	$\beta=1/2$	41.50	38.27	35.96	34.24	32.43	31.08	29.42	23.13	13.39
	$\beta=5/8$	41.50	38.27	35.96	34.16	32.43	30.68	29.37	25.30	13.46
	$\beta=3/4$	41.50	38.27	35.96	33.73	32.30	30.63	28.84	25.30	13.46
	$\beta=7/8$	41.50	38.27	35.96	33.73	32.30	30.31	28.73	25.36	13.45
7×7	$\beta=1/8$	41.77	38.56	36.12	34.35	32.63	31.04	29.59	27.61	20.34
	$\beta=1/4$	41.77	38.56	36.12	34.40	32.66	31.04	29.60	27.67	20.35
	$\beta=3/8$	41.77	38.56	36.12	34.37	32.66	31.15	29.60	27.67	20.35
	$\beta=1/2$	41.77	38.56	36.12	34.37	32.50	31.15	29.59	27.70	20.73
	$\beta=5/8$	41.77	38.56	36.12	34.30	32.50	30.73	29.54	27.51	20.80
	$\beta=3/4$	41.77	38.56	36.12	33.82	32.36	30.68	28.88	27.49	20.80
	$\beta=7/8$	41.77	38.56	36.12	33.82	32.36	30.35	28.70	27.38	21.08
9×9	$\beta=1/8$	41.96	38.70	36.18	34.37	32.63	31.05	29.58	27.70	24.28
	$\beta=1/4$	41.96	38.70	36.18	34.42	**32.67**	31.05	**29.61**	27.73	24.33
	$\beta=3/8$	41.96	38.70	36.18	34.40	**32.67**	**31.16**	29.59	27.74	24.33
	$\beta=1/2$	41.96	38.70	36.18	34.40	32.48	**31.16**	29.59	27.73	24.66
	$\beta=5/8$	41.96	38.70	36.18	34.30	32.48	30.74	29.53	27.43	24.70
	$\beta=3/4$	41.96	38.70	36.18	33.82	32.21	30.69	28.88	27.40	24.70
	$\beta=7/8$	41.96	38.70	36.18	33.82	32.12	30.36	28.70	27.28	24.66
11×11	$\beta=1/8$	41.92	**38.76**	**36.23**	34.38	32.62	31.05	29.58	27.71	25.07
	$\beta=1/4$	41.92	**38.76**	**36.23**	**34.43**	32.65	31.05	29.61	**27.75**	25.13
	$\beta=3/8$	41.92	**38.76**	**36.23**	34.41	32.65	**31.16**	29.59	**27.75**	25.13
	$\beta=1/2$	41.92	**38.76**	**36.23**	34.41	32.47	**31.16**	29.59	27.74	25.25
	$\beta=5/8$	41.92	**38.76**	**36.23**	34.31	32.47	30.74	29.53	27.45	**25.29**
	$\beta=3/4$	41.92	**38.76**	**36.23**	33.83	32.18	30.69	28.88	27.44	**25.29**
	$\beta=7/8$	41.92	**38.76**	**36.23**	33.83	32.10	30.36	28.70	27.32	25.18
13×13	$\beta=1/8$	**41.99**	38.74	36.21	34.37	32.62	31.04	29.56	27.69	25.09
	$\beta=1/4$	**41.99**	38.74	36.22	34.41	32.64	31.04	29.58	27.73	25.15
	$\beta=3/8$	**41.99**	38.74	36.22	34.35	32.64	31.15	29.55	27.74	25.15
	$\beta=1/2$	**41.99**	38.74	36.20	34.35	32.47	31.15	29.55	27.72	25.25
	$\beta=5/8$	**41.99**	38.74	36.20	34.23	32.46	30.72	29.48	27.41	**25.29**
	$\beta=3/4$	**41.99**	38.74	35.90	33.76	32.18	30.67	28.80	27.39	**25.29**
	$\beta=7/8$	**41.99**	38.74	35.52	33.76	32.10	30.33	28.62	27.29	25.18

Table 5
Denoising performances of ASMF-DBER II for different detection window size and β.

Noise	Density	10%	20%	30%	40%	50%	60%	70%	80%	90%
5×5	$\beta=1/8$	41.77	38.29	35.87	33.87	32.31	30.63	28.38	22.67	13.23
	$\beta=1/4$	41.77	38.29	35.87	33.89	32.34	30.63	28.39	22.70	13.23
	$\beta=3/8$	41.77	38.29	35.87	33.78	32.34	30.70	28.90	22.70	13.26
	$\beta=1/2$	41.77	38.29	35.87	33.78	32.17	30.70	28.91	22.75	13.26
	$\beta=5/8$	41.77	38.29	35.87	33.66	32.17	30.40	28.90	24.82	13.32
	$\beta=3/4$	41.77	38.29	35.87	33.26	32.08	30.35	28.49	24.82	13.32
	$\beta=7/8$	41.77	38.29	35.87	33.26	32.08	30.18	28.40	24.95	13.65
7×7	$\beta=1/8$	42.04	38.56	36.11	34.09	32.53	30.98	29.44	27.45	19.78
	$\beta=1/4$	42.04	38.56	36.11	34.11	32.56	30.99	29.44	27.51	19.78
	$\beta=3/8$	42.04	38.56	36.11	34.00	32.56	31.00	29.35	27.51	19.78
	$\beta=1/2$	42.04	38.56	36.11	34.00	32.38	31.00	29.35	27.51	20.18
	$\beta=5/8$	42.04	38.56	36.11	33.86	32.38	30.62	29.32	27.41	20.24
	$\beta=3/4$	42.04	38.56	36.11	33.44	32.27	30.57	28.76	27.40	20.24
	$\beta=7/8$	42.04	38.56	36.11	33.44	32.27	30.19	28.64	27.31	21.50
9×9	$\beta=1/8$	42.13	38.73	36.24	34.16	32.58	31.04	29.49	27.60	24.56
	$\beta=1/4$	42.13	38.73	36.24	34.18	32.62	31.04	29.49	27.64	24.60
	$\beta=3/8$	42.13	38.73	36.24	34.06	32.62	31.06	29.40	27.65	24.60
	$\beta=1/2$	42.13	38.73	36.24	34.06	32.43	31.05	29.39	27.64	24.86
	$\beta=5/8$	42.13	38.73	36.24	33.93	32.43	30.66	29.37	27.46	24.93
	$\beta=3/4$	42.13	38.73	36.24	33.50	32.32	30.62	28.79	27.44	24.93
	$\beta=7/8$	42.13	38.73	36.24	33.50	32.32	30.22	28.64	27.35	24.88
11×11	$\beta=1/8$	42.15	38.77	**36.27**	34.18	32.61	31.05	**29.50**	27.60	24.97
	$\beta=1/4$	42.15	38.77	**36.27**	**34.20**	**32.64**	31.06	**29.50**	**27.65**	25.01
	$\beta=3/8$	42.15	38.77	**36.27**	34.09	**32.64**	**31.07**	29.41	**27.65**	25.01
	$\beta=1/2$	42.15	38.77	**36.27**	34.09	32.45	31.06	29.40	27.64	25.12
	$\beta=5/8$	42.15	38.77	**36.27**	33.95	32.45	30.68	29.38	27.46	**25.17**
	$\beta=3/4$	42.15	38.77	**36.27**	33.52	32.34	30.63	28.79	27.44	**25.17**
	$\beta=7/8$	42.15	38.77	**36.27**	33.52	32.34	30.24	28.67	27.35	25.09
13×13	$\beta=1/8$	**42.20**	**38.79**	**36.27**	34.19	32.60	31.05	**29.50**	27.60	24.97
	$\beta=1/4$	**42.20**	**38.79**	**36.27**	**34.20**	32.63	31.06	**29.50**	**27.65**	25.01
	$\beta=3/8$	**42.20**	**38.79**	**36.27**	34.09	32.63	**31.07**	29.41	**27.65**	25.01
	$\beta=1/2$	**42.20**	**38.79**	**36.27**	34.09	32.44	31.06	29.41	27.64	25.12
	$\beta=5/8$	**42.20**	**38.79**	**36.27**	33.96	32.44	30.68	29.36	27.46	25.16
	$\beta=3/4$	**42.20**	**38.79**	**36.27**	33.52	32.33	30.63	28.71	27.45	25.16
	$\beta=7/8$	**42.20**	**38.79**	**36.27**	33.52	32.33	30.24	28.54	27.36	25.09

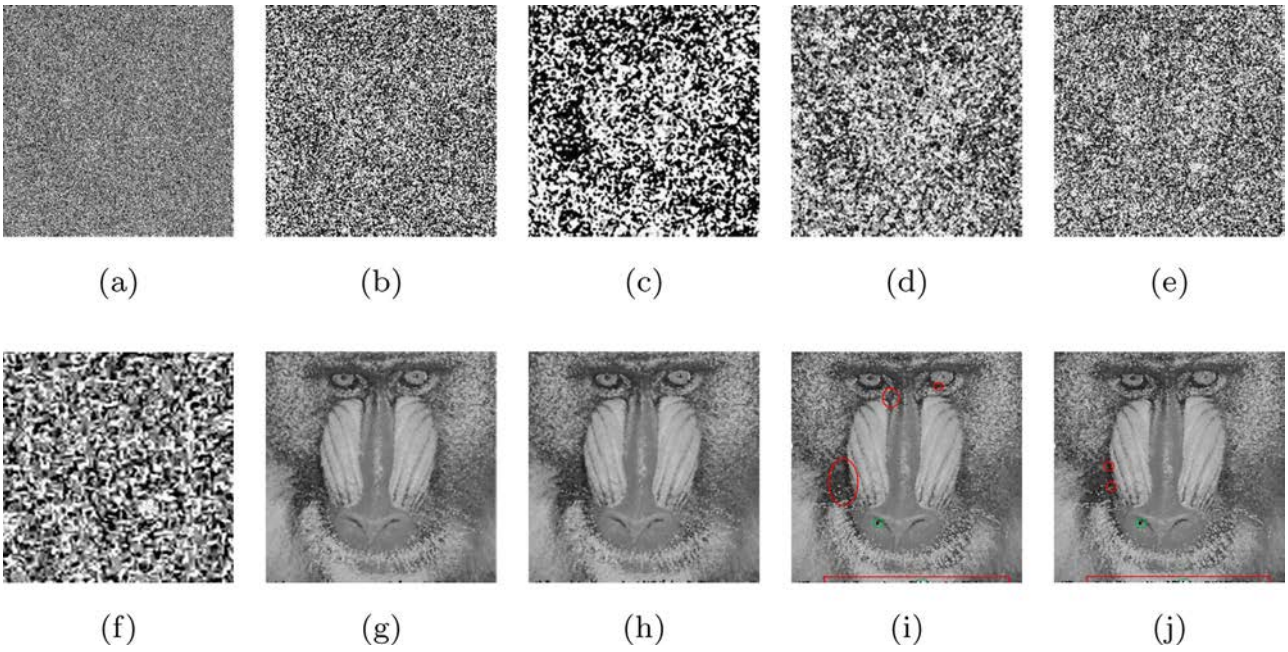

Fig. 19. Denoising results for Baboon image (noise density is 90%). (a) Corrupted image. (b) ASWM. (c) ROR-NLM. (d) BDND. (e) IBDND. (f) WCSR. (g) ASMF-DBER I. (h) ASMF-DBER II. (i) Colored detection results of ASMF-DBER I. (j) Colored detection results of ASMF-DBER II. (For interpretation of the references to colour in this figure legend, the reader is referred to the web version of this article.)

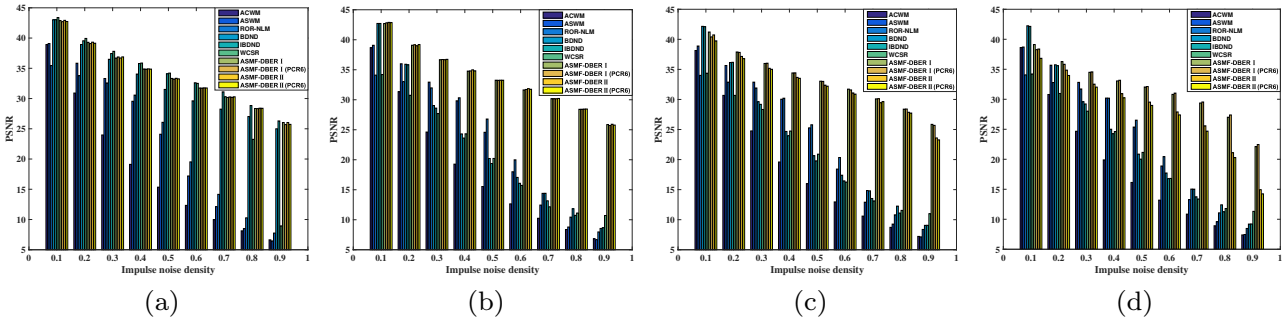

Fig. 20. Comparisons of denoising performance using PSNR for Lena images corrupted by the impulse noise with various values of α. (a) $\alpha = 0$. (b) $\alpha = 5$. (c) $\alpha = 15$. (d) $\alpha = 20$.

Table 6
Average execution time of eight algorithms for corrupted Lena image with different noise densities (unit second).

Methods	10%	20%	30%	40%	50%	60%	70%	80%	90%
ACWM	3.0	3.0	3.0	3.0	3.0	3.0	3.0	3.0	3.0
ASWM	27.9	28.9	29.3	29.4	36.7	37.5	44.1	50.3	63.2
ROR-NLM	68.5	84.5	100.1	115.7	131.5	144.2	151.0	147.2	137.6
BDND	75.6	74.7	74.9	75.5	75.9	76.6	77.5	77.4	77.7
IBDND	75.8	75.0	74.4	76.0	76.2	76.7	77.2	76.9	77.2
WCSR	3281.3	3288.5	3297.8	3293.3	3328.3	3298.6	3312.7	3326.0	3219.6
ASMF-DBER I	87.8	88.4	95.7	98.5	101.3	111.3	111.5	124.9	126.3
ASMF-DBER II	88.3	88.8	96.3	99.2	102.0	113.1	114.0	125.4	127.1

5.5. Computational cost

The computational cost is an important index to evaluate an algorithm. We timed the computational costs of ACWM, ASWM, ROR-NML, BDND, IBDND, WCSR and the proposed methods by running the algorithms on a Windows 7 Enterprise system equipped with Intel Core i7-4790 CPU at 3.60 GHz and 8.00GB DDR-III memory. The comparison of their average execution time for corrupted Lena images with size of 512×512 are shown in Table 6. Each average execution time is calculated from 10 runs of experiments. According to Table 6, the computational cost of the proposed methods varies from 80 to 130 s with the increase of noise density. The sparse representation based method WCSR is most time consuming (more than 3000 s) and the proposed methods need more computational cost compared with ACWM, ASWM, BDND and IBDND algorithms. To some extent, the better denoising performance of the proposed methods is at the cost of more computational cost.

5.6. Adaptability for different impulse noise models

In order to further check the adaptability of ASMF-DBER for the different values of α in noise model, i.e., the different intensity ranges for impulse noise, we use PSNR for Lena images corrupted by the impulse noise with other values of α, the quantitative re-

sults are shown in Fig. 20. Furthermore, we also compare the results obtained using a recent alternative fusion rule PCR6 [37] (Proportional Conflict Redistribution rule No. 6) when combining the generated BBAs m_1 and m_2 in our ASMF-DBER I and ASMF-DBER II methods. These two results are denoted by ASMF-DBER I (PCR6) and ASMF-DBER II (PCR6) respectively.

As shown in Fig. 20, the PSNR of ASMF-DBER results are relatively high when α varies between 0 and 15. Although they drop slightly when $\alpha = 20$, they are still higher than other methods in general.

6. Conclusion

To deal with the problem of the impulse noise reduction, first, we propose two impulse noise detection methods based on evidential reasoning before filtering. Second, we design an adaptive switching median filtering method, which adaptively determines the size of filtering window according to detection results. The subjective and objective analyses from our experimental results verify that our new proposed detections approaches and related filtering algorithms have superior performance compared with existing algorithms.

The generation of BBAs is crucial in evidential reasoning, however there is no general theoretical method for BBA generation. In this paper, we use two types of BBA generation methods in evidential modeling for the uncertainties encountered in the impulse noise detection and have evaluated their performances. In future work, we will focus on other BBA generation methods, which can better depict the uncertainty encountered in the impulse noise detection. Other evidence combination rules will also be used to make comparisons. We will also do more theoretical analyses on the determination of parameters used in our algorithm. Furthermore, we will apply our impulse noise detection method to sparse representation based filtering approach to deal with more complicated noise models, such as the impulse/Gaussian mixed noise.

Acknowledgment

This work was supported by the National Natural Science Foundation of China (Nos. 61671370, 61573275), Grant for State Key Program for Basic Research of China (973) (No. 2013CB329405), Science and Technology Project of Shaanxi Province (No. 2013KJXX-46), Postdoctoral Science Foundation of China (No. 2016M592790), and Fundamental Research Funds for the Central Universities (No. xjj2014122, xjj2016066).

References

[1] R.C. Gonzalez, R.E. Woods, Digital Image Processing, Prentice-Hall, 2002.
[2] J. Dezert, Z. Liu, G. Mercier, Edge detection in color images based on dsmt, in: IEEE Information Fusion (FUSION), Chicago, 2011, pp. 1–8.
[3] Z. Zhang, D. Han, Y. Yang, Image segmentation based on evidential Markov random field model, in: IEEE International Conference on Control, Automation and Information Sciences, Changshu, 2015, pp. 239–244.
[4] Y. Wang, L. Deng, Modeling object recognition in visual cortex using multiple firing k-means and non-negative sparse coding, Signal Process. 124 (2016) 198–209.
[5] F. Nellro, M.J. Thurley, H. Jonsson, C. Andersson, Automated measurement of sintering degree in optical microscopy through image analysis of particle joins, Pattern Recognit. 48 (11) (2015) 3451–3465.
[6] M.S. Zarchi, R.T. Tan, C.V. Gemeren, A. Monadjemi, R.C. Veltkamp, Understanding image concepts using ISTOP model, Pattern Recognit 53 (2016) 174–183.
[7] I. Pitas, A.N. Venetsanopoulos, Order statistics in digital image processing, Proc. IEEE 80 (12) (1992) 1893–1921.
[8] D.R.K. Brownrigg, The weighted median filter, Commun. ACM 27 (8) (1984) 807–818.
[9] S.J. Ko, Y.H. Lee, Center weighted median filters and their applications to image enhancement, IEEE Trans. Circuits Syst. 38 (9) (1991) 984–993.
[10] T. Sun, Y. Neuvo, Detail-preserving median based filters in image processing, Pattern Recognit. Lett. 15 (4) (1994) 341–347.
[11] M. Elad, Sparse and Redundant Representations: From Theory to Applications in Signal and Image Processing, Prentice-Hall, 2010.
[12] M. Aharon, M. Elad, A. Bruckstein, rmK-SVD: an algorithm for designing overcomplete dictionaries for sparse representation, IEEE Trans. Signal Process. 54 (11) (2006) 4311–4322.
[13] M. Elad, M. Aharon, Image denoising via sparse and redundant representations over learned dictionaries, IEEE Trans. Image Process. 15 (12) (2006) 3736–3745.
[14] S. Wang, Y. Xia, Q. Liu, P. Dong, D.D. Feng, J. Luo, Fenchel duality based dictionary learning for restoration of noisy images, IEEE Trans. Image Process. 22 (12) (2013) 5214–5225.
[15] S. Wang, Q. Liu, Y. Xia, et al, Dictionary learning based impulse noise removal via l1-l1 minimization, Signal Process. 93 (9) (2013) 2696–2708.
[16] S. Xu, X. Yang, S. Jiang, A fast nonlocally centralized sparse representation algorithm for image denoising, Signal Process. 131 (2017) 99–112.
[17] J. Liu, X. Tai, H. Huang, Z. Huan, A weighted dictionary learning model for denoising images corrupted by mixed noise, IEEE Trans. Image Process. 22 (3) (2013) 1108–1120.
[18] P.-E. Ng, K.-K. Ma, A switching median filter with boundary discriminative noise detection for extremely corrupted images, IEEE Trans. Image Process. 15 (6) (2006) 1506–1516.
[19] I.F. Jafar, R.A. AlNa'mneh, K.A. Darabkh, Efficient improvements on the BDND filtering algorithm for the removal of high-density impulse noise, IEEE Trans. Image Process. 22 (3) (2013) 1223–1232.
[20] T. Chen, H. Wu, Adaptive impulse detection using center-weighted median filters, IEEE Signal Process. Lett. 8 (1) (2001) 1–3.
[21] Y. Dong, S. Xu, A new directional weighted median filter for removal of random-valued impulse noise, IEEE Signal Process. Lett. 14 (3) (2007) 193–196.
[22] U. Ghaneker, A.K. Singh, R. Pandey, A contrast enhancement-based filter for removal of random valued impulse noise, IEEE Signal Process. Lett. 17 (1) (2010) 47–50.
[23] S. Akkoul, R. Ledee, R. Leconge, A new adaptive switching median filter, IEEE Signal Process. Lett. 17 (6) (2010) 587–590.
[24] C. Chen, L. Liu, L. Chen, Y. Tang, Y. Zhou, Weighted couple sparse representation with classified regularization for impulse noise removal, IEEE Trans. Image Process. 24 (11) (2013) 4014–4026.
[25] B. Xiong, Z. Yin, A universal denoising framework with a new impulse detector and nonlocal means, IEEE Trans. Image Process. 21 (4) (2012) 1663–1675.
[26] H.L. Eng, K.K. Ma, Noise adaptive soft-switching median filter, IEEE Trans. Image Process. 10 (2) (2001) 1663–1675.
[27] Z. Zhou, Cognition and removal of impulse noise with uncertainty, IEEE Trans. Image Process. 21 (7) (2012) 3157–3167.
[28] G. Shafer, A Mathematical Theory of Evidence, Princeton University Press, 1976.
[29] R. Garnett, T. Huegerich, C. Chui, W. He, A universal noise removal algorithm with an impulse detector, IEEE Trans. Image Process. 14 (11) (2005) 1747–1754.
[30] T.L. Tan, A. Pearce, T. Carter, A. Holt, Probability, Random Variables, and Stochastic Processes, McGraw-Hill, 2002.
[31] Y. Yang, D. Han, A new distance-based total uncertainty measure in the theory of belief functions, Knowl. Based Syst. 94 (2016) 114–123.
[32] P. Smets, The transferable belief model, Artif. Intell. 66 (2) (1994) 191–234.
[33] D. Han, J. Dezert, Z. Duan, Evaluation of probability transformations of belief functions for decision making, IEEE Trans. Syst. Man Cybern. 46 (1) (2016) 93–108.
[34] J.M. Tacnet, J. Dezert, Cautious OWA and evidential reasoning for decision making under uncertainty, in: IEEE International Conference on Information Fusion, Chicago, 2011, pp. 2074–2081.
[35] A. Irpino, R. Verde, Dynamic clustering of interval data using a wasserstein-based distance, Pattern Recognit. Lett. 29 (11) (2008) 1648–1658.
[36] J. Dezert, Autonomous Navigation with Uncertain Reference Points Using the PDAF, in: Multitarget-Multisensor Tracking: Applications and Advances, 2, 1991, pp. 271–324.
[37] F. Smarandache, J. Dezert, Advances and Applications of DSmT for Information Fusion : Collected Works, Rehoboth, 2004.